



**Luís Pedro Leitão  
Menezes**

**Reconstrução de Crânios Fragmentados e Avaliação  
de Ancestralidade**

**Fragment Reconstruction and Ancestry  
Estimation of Skulls using 3D models**



**Luís Pedro Leitão  
Menezes**

**Reconstrução de Crânios Fragmentados e Avaliação  
de Ancestralidade**

**Fragment Reconstruction and Ancestry Estimation  
of Skulls using 3D models**

Dissertação apresentada à Universidade de Aveiro para cumprimento dos requisitos necessários à obtenção do grau de Mestre em Engenharia de Computadores e Telemática, realizada sob a orientação científica do Professor Doutor Paulo Miguel de Jesus Dias, Professor Auxiliar, e da Professora Doutora Maria Beatriz Alves de Sousa Santos, Professora Associada com Agregação do Departamento de Eletrónica, Telecomunicações e Informática da Universidade de Aveiro.



**o júri / the jury**

presidente / president

Prof. Doutor Joaquim João Estrela Ribeiro Silvestre Madeira  
Professor Auxiliar do Dep. de Eletrónica, Telecomunicações e Informática da Universidade de Aveiro

vogais / examiners committee

Prof. Doutora Maria Beatriz Duarte Pereira do Carmo  
Professora Auxiliar da Faculdade de Ciências da Universidade de Lisboa

Prof. Doutor Paulo Miguel de Jesus Dias  
Professor Auxiliar do Dep. de Eletrónica, Telecomunicações e Informática da Universidade de Aveiro



**agradecimentos /  
acknowledgements**

I would like to thank my supervisors in this dissertation, Paulo Miguel de Jesus Dias and Maria Beatriz de Sousa Santos for their invaluable advice and guidance. I would like to extend my gratitude to the anthropologists, Catarina Coelho, Maria Teresa Ferreira, Sofia Wasterlain, João Coelho e David Navega for their collaboration and feedback. Finally, I would like to thank my friends and family for their constant support.



**palavras-chave**

Craniometria, Modelos 3D, Estruturas 3D, Classificação de Ancestralidade, Reconstrução de Fragmentos.

**resumo**

Em escavações arqueológicas é comum recuperarem-se restos osteológicos humanos fragmentados, nomeadamente os crânios. É o principal objetivo desta dissertação estudar métodos para criar uma reconstrução usando modelos tridimensionais (3D) que permita o estudo antropológico de crânios fragmentados. Este trabalho pretende também melhorar a aplicação CraMs, Craniometric Measurements, integrando funcionalidades para reconstrução de crânios fragmentados e novos métodos de classificação da ancestralidade baseados em análise estatística. Esta aplicação foi inicialmente desenvolvida com o objetivo de auxiliar o trabalho dos antropólogos na realização de medidas craniométricas e, com base em modelos 3D dos espécimes, permite reduzir a variabilidade nas medidas obtidas pelos diferentes especialistas ajudando simultaneamente na preservação dos espécimes. O trabalho desenvolvido nesta dissertação está focado na reconstrução de espécimes que estão num estado fragmentado para serem posteriormente analisados na aplicação CraMs, o que era previamente não era possível. Foram também desenvolvidos métodos que permitem o armazenamento centralizado de análises feitas pelos antropólogos e a sua utilização para estimar a ancestralidade de um indivíduo usando análise estatística.





**keywords**

Craniometry, 3D models, 3D Structures, Ancestry Classification, Fragment Reconstruction.

**abstract**

In archaeological sites, it is common to find fragmented human osteological remains, namely skulls. The main goal of this dissertation is to investigate processes to create reconstructions using three dimensional models(3D) in order to allow the study of fragmented skulls. This work also aims to improve the application CraMs, Craniometric Measurements, by adding new functionality to reassemble skull fragments and expanding the ancestry classification using statistical analysis. This application was initially developed in the context of a Master dissertation with the goal of assisting the anthropologist's work in performing craniometric measurements and by using 3D models of the individuals reduce the variability in the measurements obtained by the different specialists while at the same time contributing to the preservation of the specimens. The work developed in this dissertation is focused on the reconstruction of specimens that are in a fragmented state to be later analyzed with CraMs, something which was not previously possible. Methods were also developed to allow for a centralized storage of previous analysis by anthropologists and use them to estimate the ancestry of an individual using statistical analysis.



# TABLE OF CONTENTS

---

Table of Contents .....	ii
Index of Figures .....	v
Index of tables.....	vii
1 Introduction .....	1
1.1 Motivation and Objectives .....	1
1.2 Dissertation Structure.....	2
2 Craniometry .....	3
2.1 Traditional Craniometry.....	3
2.2 Geometric Morphometrics.....	4
2.3 Data Set .....	4
2.4 3D Scanning and Skull Acquisition.....	5
3 CraMs – Craniometric Measurements.....	7
3.1 Evolution of CraMs .....	7
3.1.1 Initial Version .....	7
3.1.2 Detection of Morphological Structures .....	9
3.1.3 Geometric Analysis .....	11
3.2 Limitations .....	13
3.3 Modifications and Improvements .....	13
3.3.1 Software Issues .....	13
3.3.2 Usability Issues.....	14

3.3.3 Additional Features Implemented .....	14
4 Ancestry Estimation .....	17
4.1 3D-ID .....	17
4.2 Initial Preprocessing .....	19
4.3 Generalized Procrustes Analysis.....	20
4.3.1 Translation .....	22
4.3.2 Uniform Scaling.....	22
4.3.3 Rotation to Reference.....	22
4.3.4 Procrustes Distance .....	23
4.4 Classification .....	23
4.5 Mahalanobis Distance .....	24
4.6 Additional Metrics .....	24
5 Fragment Reconstruction .....	27
5.1 Fragment Reconstruction Algorithms.....	27
5.1.1 Fragment Classification.....	28
5.1.2 Template-Based Reassembly .....	28
5.1.3 Fracture-Based Reassembly.....	30
5.1.4 Hybrid Reassembly.....	31
5.1.5 Skull Completion .....	31
5.2 Fragment Reconstruction within CraMs.....	32
5.3 Rough Pre-Alignment.....	32
5.3.1 Early Attempts with Automatic Template Alignment.....	32
5.3.2 Semi-Automatic Alignment.....	33
5.4 Pair-wise Refinement .....	34
5.4.1 Probe Point Determination.....	35
5.4.2 Seed Point Calculation .....	37
5.4.3 Fracture Region Expansion .....	38

5.4.4 Computing and Applying Transformation.....	38
5.4.5 Semi-Automatic Region Expansion .....	39
6 Results.....	41
6.1 Ancestry Estimation.....	41
6.2 Fragment Reconstruction .....	44
7 Conclusion and Future Work .....	55
7.1 Conclusion .....	55
7.2 Future Work.....	56
References.....	59
Annex A – Crams User Manual.....	63
Annex B – Instalation Guide .....	69
Annex C – Points of Interest.....	73
Annex D – Craniometric Measures.....	79

# INDEX OF FIGURES

---

Figure 1 – Acquired 3D models of the two fragments from an autopsied individual used in the Fragment Reconstruction Process. ....	5
Figure 2 - Breuckmann SmartSCAN 3D Scanner. Image taken from (Santos, 2014).....	6
Figure 3 – NextEngine 3D Laser Scanner during operation. Image taken from (Andrade, 2016).....	6
Figure 4 - Application Workflow. Adapted from (Santos, 2013).....	8
Figure 5 - Orbit Structure represented with pink spheres and the corresponding reference points represented with green spheres. Taken from (Neves, 2014). ....	10
Figure 6 – Detection of Sagittal Structure. Before(top) and after (bottom) the detection process, with the initial structure represented with dark blue spheres and the points subsequently added with teal spheres. Taken from (Neves, 2014). ....	10
Figure 7 - Calculated Nasal Structure and its resulting projection. Taken from (Andrade, 2016)...	11
Figure 8 - Three different types of Anterior Nasal Spine. Taken from (Andrade, 2016).....	12
Figure 9 - Neurocranium divisions and sampling. Taken from (Andrade, 2016).~ .....	12
Figure 10 – Small segment of the craniometric database. ....	15
Figure 11 - Flowchart of the Generalized Procrustes Analysis algorithm used in the Ancestry Estimation process. ....	21
Figure 12- Keypoint detection and matching for Template Based Reassembly. Taken from (Zhang, 2015). ....	29
Figure 13 – On the left curvature information, on the right the resulting MST. Taken from (Pauly et al, 2003).....	30
Figure 14– Template-based skull completion. Taken from (Wei, 2011).....	31
Figure 15 – Problems with excessive false positive correspondences using Template-Based alignment. ....	33

Figure 16 - The pair-wise alignment processes with green spheres representing the points selected on each and the light blue lines joining corresponding points. On the left is the alignment between fragments and a template and on the right the alignment solely between fragments. .... 34

Figure 17 - Workflow for the Pair-wise Alignment refinement. .... 35

Figure 18- On the left is a side view of two neighboring fragments with their centers of mass represented by red spheres, the middle plane perpendicular to line between them in orange and the probe points in yellow. On the right is a top down view of the probe point represented as yellow sphere organized as a rectangle with its center as a green sphere. .... 36

Figure 19 - View of the 150 candidate points for each probe point on each fragment (green spheres) with the selected seed points (blue spheres) and the corresponding seed points joined by a light blue line. .... 37

Figure 20 - Expanded fracture region in purple generated from the seed points seen as blue spheres. The red sphere represents the center of mass of the fragment. .... 38

Figure 21 – On the left the fragments before the reconstruction and on the right the resulting reconstructed skull. .... 39

Figure 22 – Representation of the distribution of reconstructions by classification given by the anthropologists. .... 52

Figure 23 - Problems detecting the fracture region in calvarium areas perpendicular to the probe planes on individual 74. .... 52

Figure 24 - Average Fracture distance of the individual of each classification value. .... 53



# INDEX OF TABLES

---

Table 1 – Craniometric points not used in CraMs added to accommodate the 3D-ID database and their definition. Adapted from (Slice & Ross, 2009). .....	19
Table 2 – Points used to test the Ancestry Estimation process for each individual. The abbreviations of the point names follow the rules described in Annex 1. ....	42
Table 3 - Results of Ancestry Estimation applied to the individuals with points marked by the antropologists using CraMs and 3D-ID marked with green when correctly identified and red when otherwise. ....	43
Table 4– Results of the Reconstruction comparison between the physical reconstruction and the one done using CraMs using Basion-Bregma Height measurements. ....	45
Table 5 – Results of visual classification done by the antropologists and average fracture distance of the reconstruction done using CraMs. ....	51

# 1 INTRODUCTION

---

## 1.1 Motivation and Objectives

The CraMs, Craniometric Measures, application is a tool developed to enable digital craniometric analysis of skulls using their acquired three-dimensional (3D) models. This application has been constantly evolving in recent years with its development done in the context of three Master dissertations between 2012-2016 (Andrade, 2016; Neves, 2014; Santos, 2013). The CraMs application focuses on emulating the craniometric analysis that was traditionally done by hand using 3D models in a computer system and enhancing it by reducing the inaccuracy and lack of repeatability associated with human interaction. The work presented here aims to expand the CraMs's capabilities by enabling the ability to reconstruct fragmented skulls and adding a new type of Ancestry Estimation process using comparisons with a large dataset.

An initial meeting was held with the anthropologists to evaluate the current state of CraMs and the ways in which it could be enhanced. During this meeting the experts expressed that the large majority of cranial remains recovered are fragmented into multiple pieces and are often difficult or even impossible to reconstruct, which poses difficulties in obtaining craniometric measures. A process to digitally reconstruct these fragments, making them then able to take advantage of the full CraMs toolset (calculating craniometric measures, structures, etc.) was to be prioritized. Additionally, the anthropologists wanted to expand the Ancestry Estimation tool in the application to use multivariate analysis methods on a craniometric point database, in a process similar to that

of 3D-ID<sup>1</sup>, a tool they regularly use. After reading through the previous dissertations and examining the feedback received from the anthropologist team during the meeting it also was evident that some components of the application required some improvement and modifications to be better suited for everyday usage.

## **1.2 Dissertation Structure**

This dissertation is organized in seven chapters, starting with this chapter that contains a brief introduction to the work developed.

Chapter 2 presents a description of traditional Craniometry, geometric Morphometrics, the data sets that were used as well as the 3D scanning acquisition process

Chapter 3 provides some information about the evolution of the CraMs application, its current state and the functional and interface issues that were addressed.

Chapter 4 describes the concepts and methods implemented in the Ancestry Estimation process.

Chapter 5 focuses on the skull fragment reconstruction and the processes used to achieve it.

Chapter 6 presents the main results obtained and their discussion.

Finally, Chapter 7 presents the conclusion as well as possible future work.

---

<sup>1</sup> <http://www.3d-id.org/>

# 2 CRANIOMETRY

---

This chapter presents the concepts and tools used by anthropologists in the field of Craniometry and Geometric Morphometrics. Additionally the data set is presented as well as a brief description of 3D scanning acquisition processes used. Further detail on these topics can be found in the previous Master dissertations (Andrade, 2016; Neves, 2014; Santos, 2013).

## 2.1 Traditional Craniometry

Craniometry is the study of human cranial measurements to establish anthropological comparisons and classifications between multiple individuals (Stephens, 2000). Craniometry is widely used in Anthropology to evaluate ancestry, sex and human evolution in populations (Buck & Vidarsdottir, 2004; Howells, 1973; Stephens, 2000).

Traditional Craniometry is done by measuring distances between a pair of landmark points, points on the skull of anatomical importance, through the use of specialized tools and the physical manipulation of the skulls (Stephens, 2000). The exact location of these landmark points however, relies on visual and tactile assessments, which can result in slight variations between different anthropologists (Inter-Observer error), or even the same anthropologist at different moments (Intra- Observer Error) due to their subjective nature. These landmark points can also be used to classify and unknown individual's ancestry and sex, by observing the relations between them. This can be achieved by taking a set points from an individual and comparing them to point sets

representative of an ancestry/sex group and find the closest match, a process that will be explained later on in this dissertation.

## **2.2 Geometric Morphometrics**

The analysis of the shape and size of a cranial remains, a concept that encompasses size and shape is called Geometric Morphometrics. When analyzing the geometry of a morphological structure, landmarks can be defined, not only by points but by shape, volume or even curvature. These concepts have various application like performing ancestry classifications by determining the closest template shapes (Hefner, 2009) or gender classification based on the shape of the neurocranium like the one used by (Andrade, 2016). In the context of this dissertation morphometric analysis is used to identify and match correspondent fracture regions on fragmented individuals, the areas on each piece created by the fragmentation, based on curvature values to produce the geometric optimal transformation for a subsequent reconstruction.

## **2.3 Data Set**

The data set is composed by two collections. The first one is the same used by Santos (2013) from an excavation performed at the Vale da Gafaria (Leprosarium Valley), outside the city of Lagos in Portugal (Wasterlain SN, Neves MJ, 2016) by the iDryas team. The excavation site, active between the 15th and 17th centuries revealed two occupations.

The second collection come through a collaboration between Department of Life Sciences, University of Coimbra, and the City Council of Santarém established in 2009 enabling the acquisition of non-claimed skeletal remains from the Capuchos cemetery (Ferreira et al., 2014) . This set of remains, called 21<sup>st</sup> Century Identified Skeletal Collection (CEI/XXI), is composed of skeletons originated from the sampling of modern Portuguese unclaimed or abandoned beyond the legal time frame. This collection consists of 240 sets of skeletal remains. All the individuals are Portuguese nationals, of both sexes, with the age at death fluctuating between 29 and 99 years. The male sample set is composed of 74 individuals with ages between 25 and 95. The female sample set on the other hand has 85 individuals with a lower age at the time death distribution, the younger being 50 and the oldest 99 years old. This collection also contains the individuals whose skulls are in multiple pieces used to in the Fragment Reconstruction process. These later individuals were

subjected to autopsies and as such their skulls are divided into two pieces with the cut angle varying between them. There are 9 individuals total, 4 being females and 5 males. An example of these individuals can be seen in Figure 1.

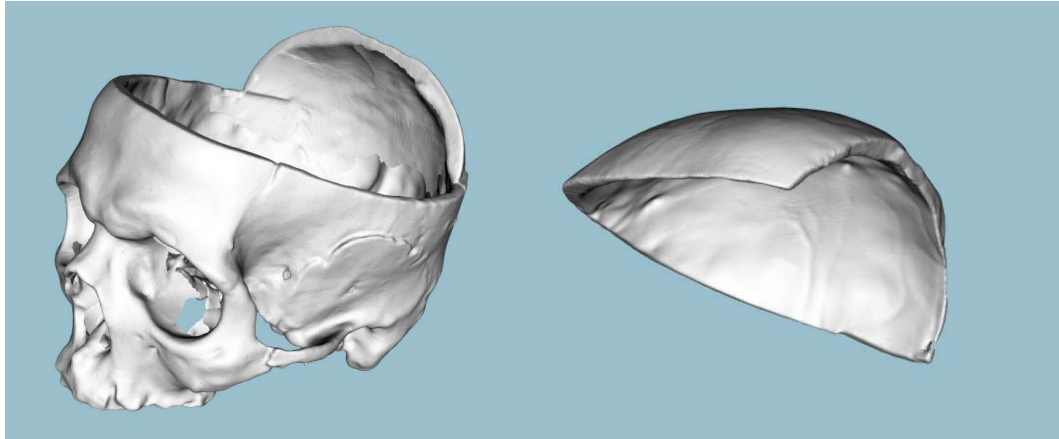


*Figure 1 – Acquired 3D models of the two fragments from an autopsied individual used in the Fragment Reconstruction Process.*

## **2.4 3D Scanning and Skull Acquisition**

Traditionally archeological and biological anthropology studies were performed by hand on the physical specimens themselves. This approach had the drawbacks that the examined specimens could be damaged or even lost during transit. With the advent of digital technologies in recent years the advantages of integrating these technologies in these fields became apparent (Balzeau et al., 2010; Wachowiak & Karas, 2009; Weber, 2013). There are various techniques for high precision three-dimensional and color information acquisition available. Although some of the techniques involve the manual handling of the specimens being scanned the scanning process itself doesn't involve any physical contact as not to damage the fragile human osteoarcheological remains.

The specimens of the collection obtained in the Vale de Gafaria excavation were acquired by the iDryas team using a structured light scanner, called Breuckmann SmartSCAN<sup>2</sup>, seen in Figure 2.

---

<sup>2</sup> <http://aicon3d.com/products/aicon-scanner/smartsan/at-a-glance.html>



*Figure 2 - Breuckmann SmartSCAN 3D Scanner. Image taken from (Santos, 2014).*

When the collaboration with iDryas ended access to the Breuckmann scanner was no longer a possibility and so subsequent acquisition was done with the NextEngine 3D Laser Scanner<sup>3</sup>, shown in Figure 3, acquired by the Science and Technology Department of the University of Coimbra. This scanner uses laser triangulation, where a series laser beams are projected onto the object and then captured by a camera to obtain depth information. The object rests on a rotating plate with the purpose of obtaining information from multiple angles which is subsequently blended together to create a 3D model.

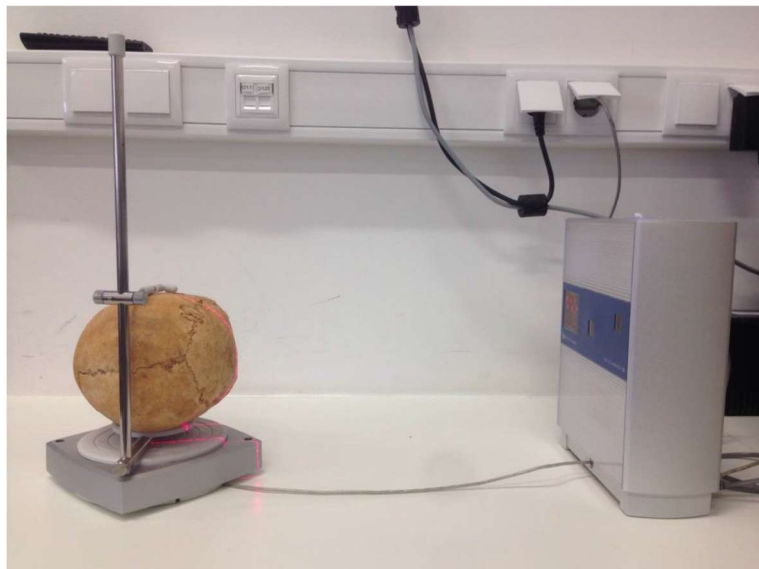


*Figure 3 – NextEngine 3D Laser Scanner during operation. Image taken from (Andrade, 2016).*

---

<sup>3</sup> <http://www.nextengine.com/>

# 3 CRAMS – CRANIOMETRIC MEASUREMENTS

---

This chapter presents the description of the application CraMs split into two main sections. The first describes the evolution of the CraMs application through its three iterations while the latter details the modifications and improvements implemented.

## 3.1 Evolution of CraMs

This section provides an overview of the different iterations of the CraMs application, presenting the main lines of the works by Santos (2013), Neves (2014) and Andrade (2016). The details of the various features added in each iteration and a brief overview of their inner workings are shown in the following sections.

### 3.1.1 Initial Version

The CraMs application was initially developed by (Santos, 2013) in the C++ programming language and using the 3<sup>rd</sup> party frameworks: Visual Toolkit (VTK)<sup>4</sup>, an open-source 3D graphics, visualization

---

<sup>4</sup> <http://www.vtk.org/>



and image processing library, to visualize and manipulate the acquired 3D models and Qt<sup>5</sup>, a framework for graphical application development, to create and manage the graphical user interface. The CraMs application, whose workflow can be seen in Figure 4, was divided into four different modules:

- GUI to manage the user interface and the window lifecycle.
- Interface to handle the manipulation of the 3D models.
- Tools encompassing the different methods of alignment and structure/point calculation.
- Utils containing the data structures used internally and additional assistant functions.

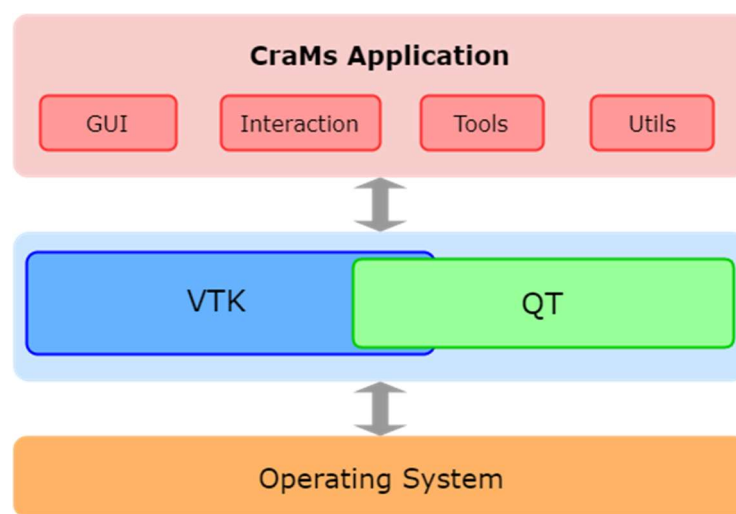


Figure 4 - Application Workflow. Adapted from (Santos, 2013).

To correctly calculate the craniometric measurements a consistent reference frame must be established through an alignment process. Two alignment methods are available:

- Manual: the alignment calculated by setting the position of seven craniometric points.
- Semi-Automatic: the alignment is calculated by applying the Iterative Closest Points (ICP) algorithm (Besl, P. J., & McKay, 1992) between the loaded model and a pre-alignment template model.

The landmark points, used to compute craniometric measurements, are obtained using one of three methods:

---

<sup>5</sup> <https://www.qt.io/>

- Manual: the point is defined completely by the user, using an interactive procedure.
- Semi-Automatic: the point is determined a combination of user input and analysis performed by the application on the neighborhood/curvature/coordinate.
- Automatic: the point is determined automatically based on pre-defined rules of minimum/maximum points on the anatomical planes (description of these planes available in (Santos, 2013)).

### 3.1.2 Detection of Morphological Structures

The second iteration of CraMs by (Neves, 2014) extended CraMs functionality by adding support for morphological structures. These structures are defined through the analysis of curvature value and type on neighboring point using a method called Region Growing (Vieira & Shimada, 2005). Given a set of reference points, manually defined by the user, the structure is created by creating a closed loop of Sharp Edges, groups of points with large values of convex curvature. The detection of two types of morphological structures was added to CraMs: Orbits and Sutures.

To detect the Orbit structure, four reference points in the orbital cavity region need to be defined by the user. The neighborhood of these points is then iteratively analyzed and points that form a sharp edge are added to the structure. Finally, the structure is filtered to select the shortest path between the reference points, with the final structure being like the one seen in Figure 5. Two additional 3rd-party libraries were added: the mathematics libraries Wild Magic<sup>6</sup> and Boost<sup>7</sup> to assist in projecting the orbit structure into a plane.

---

<sup>6</sup> <https://www.geometrictools.com/>

<sup>7</sup> <http://www.boost.org/>

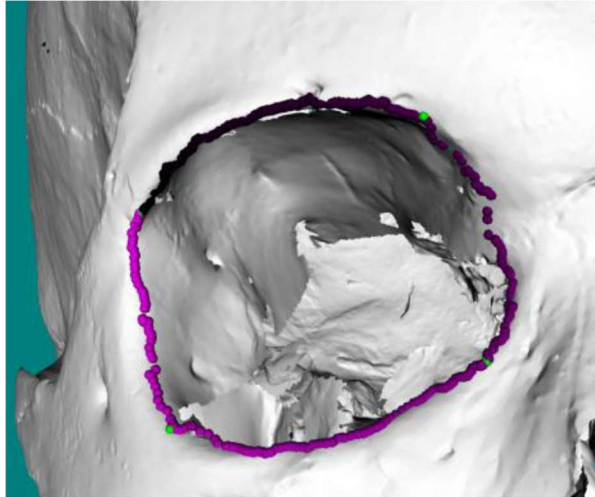


*Figure 5 - Orbit Structure represented with pink spheres and the corresponding reference points represented with green spheres. Taken from (Neves, 2014).*

For Sutures, only two reference points are required, one at each end of the structure. An initial structure is defined by the sharp edges path connecting the reference points. Subsequently, the directly connected points are analyzed repeatedly to find additional sharp edges. When no more sharp edges found or the neighborhood size maximum threshold is met, the region is cleaned up by dividing it by the number of points in the model. The resulting structure can be seen in Figure 6.

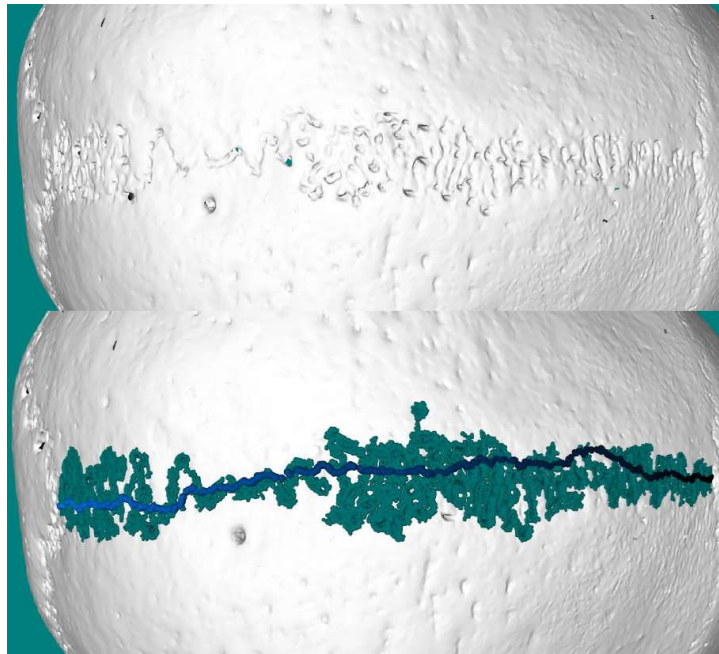


*Figure 6 – Detection of Sagittal Structure. Before(top) and after (bottom) the detection process, with the initial structure represented with dark blue spheres and the points subsequently added with teal spheres. Taken from (Neves, 2014).*

### 3.1.3 Geometric Analysis

The contributions made by (Andrade, 2016) focused on adding tools to perform morphological analysis to classify the skulls by ancestry group and sex. The foundation for this analysis was a study conducted by (Hefner, 2009) which defined eleven morphological characteristics and their correlation with population groups. Hefner created multiple templates for each characteristic that can be used to identify individuals. Some of templates for these traits can be somewhat ambiguous and so could not be automated. Support for three traits was added into CraMs: Nasal Aperture Width (NAW), PostBregmatic Depression (PBD) and Anterior Nasal Spine (ANS).

To calculate the Nasal Aperture Width nasal structure must first be defined. This is done with the same Region Growing algorithm used in the previous structures while using only two reference points. The outline is then extracted by projecting the nasal structure to a plane as can be seen in Figure 7 which is then compared to the three Hefner templates using Euclidian distance between them.

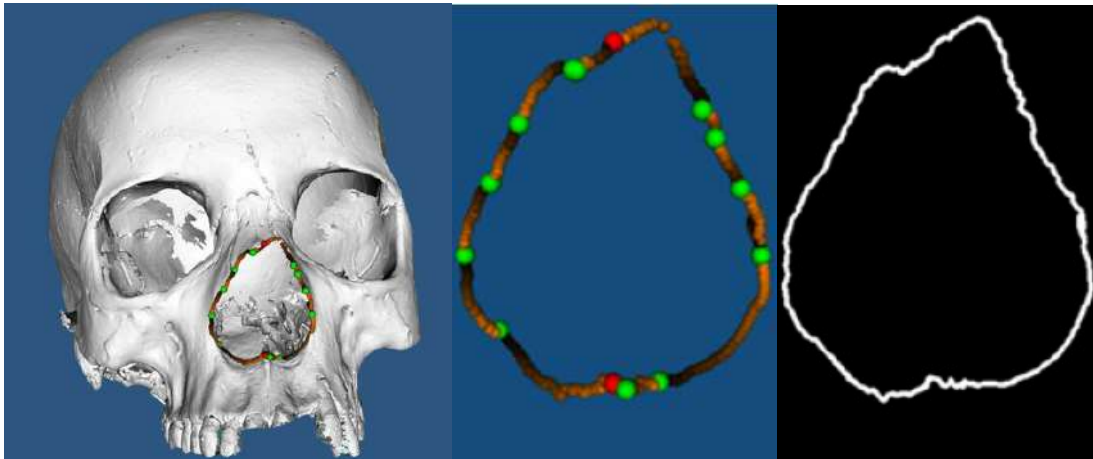


*Figure 7 - Calculated Nasal Structure and its resulting projection. Taken from (Andrade, 2016).*

The PostBregmatic Depression is computed by extracting a lateral projection of the skull and observing the segment between Bregma and the point with the highest y value. If this segment is below a straight line between these points, then the PostBregmatic depression is classified as present.

The Anterior Nasal Spine is classified by observing the points within five millimeters of the Nasospinale in a plane parallel to the z-axis and passing through it. The classification is set to slight

if the points have a more pronounced projection than the Nasospinale and differentiated from intermediate to marked base on the outcome of an equation created by (Andrade, 2016). The three types of ANS are show in Figure 8.

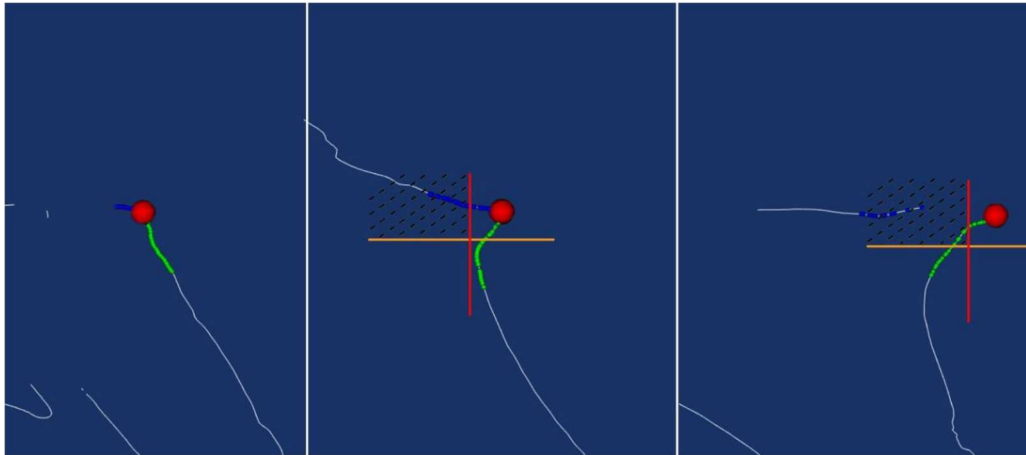


*Figure 8 - Three different types of Anterior Nasal Spine. Taken from (Andrade, 2016).*

For sex classification (Andrade, 2016) developed a method to divide the neurocranium into equidistant parts based on input by the user. The segments are then uniformly sampled so that the resulting points can be entered into 3<sup>rd</sup> party machine learning system that provides an estimate of the individual's sex. This process is shown in Figure 9.

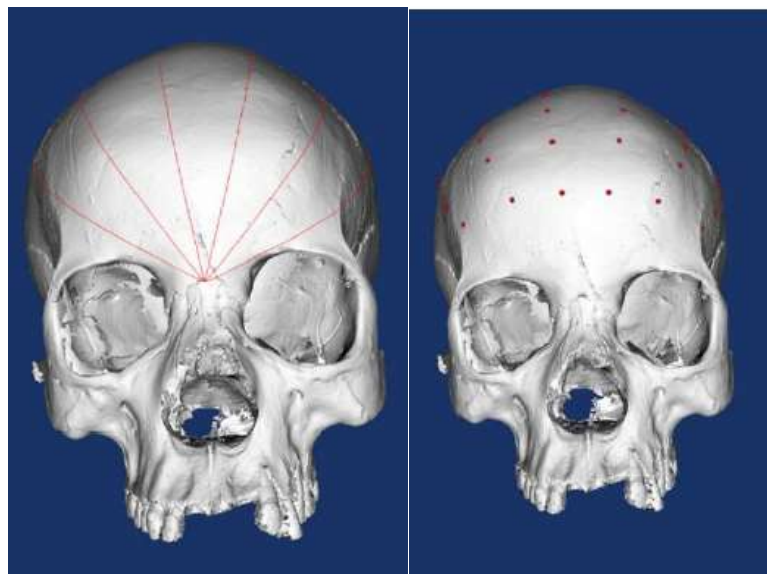


*Figure 9 - Neurocranium divisions and sampling. Taken from (Andrade, 2016).~*

## 3.2 Limitations

While using the latest version of the CraMs application the anthropologist team identified a few software and usability issues:

### Software Issues:

- The automatic points are sometimes not correctly detected.
- The application would start with the same window size regardless of the monitor resolution.

### Usability Issues:

- Left and Right Alares are not set automatically after calculation of the nasal structure and nasal\_limit points that were calculated instead were redundant.
- When marking pair of points that are Left/Right symmetrical there were no way to guarantee the symmetry relative to the Sagittal plane between them which is required by definition.

## 3.3 Modifications and Improvements

### 3.3.1 Software Issues

The automatic points would occasionally be incorrectly marked. This was caused by artifacts from the acquisition process in the form of isolated vertices away from the main model. Since the calculation of the automatic points is based on minimum/maximum values of axis or anatomic planes these points are erroneously chosen. This was fixed by limiting the ranges of values allowed to be within the range of normal skulls size to exclude these extreme values.

The window size of the CraMs application was always the same regardless of the resolution of the computer screen. This slight inconvenience was corrected by starting the CraMs window maximized and setting the interface element's size to be relative to the window size.

### **3.3.2 Usability Issues**

When detecting, the nasal structure using the method developed by Andrade (2016) the Left and Right Alares points are calculated in the form of the temporary points *left\_nasal\_limit* and *right\_nasal\_limit* respectively. This redundancy was eliminated by automatically setting the Alares value after the calculation of the nasal structure is done and removing the temporary points completely from CraMs.

Some cranial points have left/right symmetrical pairs. In the previous version of CraMs these points were marked independently meaning that there was no guarantee that they were correctly aligned relative to the sagittal plane. This could produce measurements that differ from those obtained with traditional methods because the nature of the tools used guarantee symmetry between these points. The solution to this problem was to only allow to mark these types of craniometric points in pairs. The user identifies either left or right point and the corresponding point in the pair is calculated and set automatically by finding the closest point to its symmetric relative to the Sagittal Plane.

### **3.3.3 Additional Features Implemented**

#### **Craniometric Database**

Previously the measurements taken with CraMs could be saved but they were stored in regular text files. This was not very practical because it required many files to be stored. Even worse, the anthropologists had to copy and manually maintain all these files if they wanted to keep a common pool of measurements between multiple machines. Given that one of the goals was to create an Ancestry Estimation solution based on the multivariate analysis of large amounts of point data it was imperative to organize all the point information produced with CraMs. For this reason, a craniometric point database was created integrated into the application. A system to allow users to import data from 3rd party datasets to increase the dataset and allow the Ancestry Estimation to function properly even without any data from CraMs. This database also enables an organized and condensed storage of point that could eventually be stored remotely on a server if such feature was desired.

This craniometric database was constructed using the MySQL framework. This is mainly because of its popularity throughout the industry, long standing support and ease of use. It contains only one table called “Craniometric Data” that stores point and classification data for each individual. The created table contains entries for all the cranial points used in CraMs and eleven additional points that were later added to accommodate data from the 3D-ID (see section 4.2). The points data is organized as three double precision floating point for each point as can be seen in Figure 10.

id	file_name	ancestry	ancestrygroup	gender	ϕpisthokranion_x	ϕpisthokranion_y	ϕpisthokranion_z	bregma_x	bregma_y	bregma_z	rhinion_x	rhinion_y	...
5334	IMPORT_3DID	MONGOLIAN ...	East Asian	M	-9999.0	-9999.0	-9999.0	-57.2017	234.18289999...	268.5688	-9999.0	-9999.0	...
5333	IMPORT_3DID	MONGOLIAN ...	East Asian	M	-9999.0	-9999.0	-9999.0	-120.7991	255.9744	262.538	-9999.0	-9999.0	...
5332	IMPORT_3DID	MONGOLIAN ...	East Asian	M	-9999.0	-9999.0	-9999.0	-104.3492	256.3849	266.745	-9999.0	-9999.0	...
5331	IMPORT_3DID	MONGOLIAN ...	East Asian	M	-9999.0	-9999.0	-9999.0	-90.768	275.12509999...	268.6574	-9999.0	-9999.0	...
5330	IMPORT_3DID	TOLTECAN M...	MesoAmerican	M	-9999.0	-9999.0	-9999.0	-147.5789	228.4684	265.86419999...	-9999.0	-9999.0	...
5329	IMPORT_3DID	MONGOLIAN ...	East Asian	M	-9999.0	-9999.0	-9999.0	-110.3764	247.6407	278.66309999...	-9999.0	-9999.0	...
5328	IMPORT_3DID	TOLTECAN M...	MesoAmerican	M	-9999.0	-9999.0	-9999.0	-148.8828	214.9179	265.58449999...	-9999.0	-9999.0	...

Figure 10 – Small segment of the craniometric database.

As for classification, each individual has sex and ancestry group and super-group data field as text strings. The ancestry group is the most specific ancestry classification pertaining to a small region or nationality (Portuguese, Mexican, etc.) and super-group corresponds to the broader classification (European, East-Asian, African, etc.). The ancestry groups and super-groups are dynamically added with no pre-defined limitation as to accommodate the adoption of any 3<sup>rd</sup> party databases.

### Configuration Improvements

Initially the application developed by (Santos, 2013) fully supported both Windows and Linux-based operating systems. However, during the two following iterations that ability was lost by the addition feature with no concern for cross-platform support. The portability was restored replacing Windows specific functions that control the flow of execution such as sleeps and the PDF viewer module with native C++ equivalents as these are platform independent. Additionally, the previous versions of CraMs were using outdated versions of VTK and QT libraries and could only be compiled on Visual Studio 2010. CraMs was then ported to VTK version 7.0 and QT version 5.7 by updating some functions structure following the official migration guide<sup>8</sup>. The appropriate dependency files

<sup>8</sup> [http://www.vtk.org/Wiki/VTK/VTK\\_6\\_Migration\\_Guide](http://www.vtk.org/Wiki/VTK/VTK_6_Migration_Guide)



needed to be added manually into Visual Studio one by one. This was very inconvenient and created unnecessary problems resolving eventual dependency problems for something that could be done automatically. Since the project generated already used CMake changes were made to the configuration file to link the necessary binary files using system environment variables or set the path manually as seen in Annex B.

# 4 ANCESTRY ESTIMATION

---

This chapter presents the solution created in CraMs to provide an ancestry estimation of an unknown individual: the group with similar physical and genetic characteristics to which a set of cranial remains being analyzed have a significant probability to belong to. The motivation for such process originates from the discussion with the anthropologists where it was suggested that a system to estimate the ancestry of cranial remains through statistical analysis using a large dataset could be of value to the application. The anthropologists already used a tool with this kind of functionality called 3D-ID, developed by the NCSU Forensic Laboratory in 2014. The feedback given by anthropologist was that this was a very useful tool, providing a good estimate given only a handful of craniometrics points and so would be very beneficial for their workflow to have such functionality natively within CraMS. In this chapter, the inner working of the Ancestry Estimation process used by 3D-ID will be presented as well as all the details of its implementation in the CraMs application.

## 4.1 3D-ID

The 3D-ID Ancestry Estimation process, as described in (Slice & Ross, 2009) assigns an ancestry and sex classification of an unknown individual by comparing the average distance between craniometric points with those of each ancestry and group. To establish this comparison, 3D-ID takes advantage of a large forensic database of already classified individuals to determine the mean individual for each group with at least same set craniometric points. This forensic database stores

the coordinate values for 34 cranial points and the ancestry and sex classification assigned. It contains data from the cranial remains of 1089 individuals gathered from various forensic laboratories and museums. The majority of the individuals in the database is from African American and European American ancestry. Only a subset of this database is publicly available totaling 889 individuals.

The first step in the 3D-ID process is to validate the 3D coordinates of cranial points of the unknown subject. Since these point coordinates are entered by the user this validation serves to ignore points that don't have numeric values for each of the three coordinate components. Additionally, for a direct comparison to be established the forensic database must be filtered to obtain only the individuals that have at least all the same points as the Unknown.

Several factors can interfere with the results of a comparison based on geometric similarity namely differences in size, orientations and coordinate. To mitigate this 3D-ID applies a superimposing algorithm called Generalized Procrustes Analysis (Gower, 1975). This algorithm iteratively attempts to align sets of points to their mean until convergence is achieved. This is necessary to establish a common reference frame so that a correct comparison can be made between the Unknown and all the different groups.

Finally, the difference between the sets of craniometric points from the unknown subject and the average of each of the ancestry and sex groups is computed using the Mahalanobis Distance (Orlov, 2011), an algorithm to calculate the geometric distance between an element and a distribution. The ancestry group with the lowest distance is used as the classification attributed to the unknown individual. Since the distances between the Unknown and multiple groups might be very similar, two additional metrics are calculated to increase the reliability of the classification process: Posterior Probability and a custom created "typicality" measure.

The method for ancestry estimation implemented in the CraMs application was identical to the one used in 3D-ID. It is divided into three phases: an initial preprocessing where the database is filtered for individuals with the required cranial points, the superposition of the groups using Generalized Procrustes Analysis and finally the tested skull is classified and the additional metrics are calculated.

## 4.2 Initial Preprocessing

As mentioned in section 3.3.3 a database was created to store the point data and classifications from analysis done using CraMs and data from obtained external sources. The publicly available database used by 3D-ID was then imported to attempt to obtain similar accuracy, and to function as starting point to be expanded upon with data added using CraMs. This database contains all cranial points that were already being used within CraMs as well as the 11 cranial points that 3D-ID uses but were not present, as seen in Table 1.

*Table 1 – Craniometric points not used in CraMs added to accommodate the 3D-ID database and their definition. Adapted from (Slice & Ross, 2009).*

<b>Craniometric Point</b>	<b>Definition</b>
Left Asterion	Intersection of left parietal, left temporal, and occipital bones. If sutures are indistinct or include wormian bones, project suture lines until they intersect.
Right Asterion	Intersection of right parietal, right temporal, and occipital bones. If sutures are indistinct or include wormian bones, project suture lines until they intersect.
Left Frontomolare Anterior	Left side of skull: most anterior projecting point on the frontomolare suture (different from the Frontomolare orbitale and temporale).
Right Frontomolare Anterior	Right side of the skull: most anterior projecting point on the fronto-molare suture (different from the Frontomolare orbitale and temporale).
Left Mastoidale	Left mastoid process: point is located on the inferior end.
Right Mastoidale	Right mastoid process: point is located on the inferior end.
Left Nasomaxillary Suture Pinch	Narrowest portion of the midline of the face to the left naso-maxillary suture. The minimum distance between wnbl-wnbr forms the simotic chord.
Left Nasomaxillary Suture Pinch	Narrowest portion of the midline of the face to the right naso-maxillary suture. The minimum distance betweenwnbl-wnbr forms the simotic chord.
Supspinale	The deepest point of the profile below the anterior nasal spine.
Left Zygoorbitale	Left eye orbit: point of intersection between zygomaxillary suture and eye orbit.
Right Zygoorbitale	Right eye orbit: point of intersection betweenzygomaxillary suture and orbit border.

Additionally, each entry also contains the following data fields:

- Origin of the data, whether it came from CraMs or was imported from a third-party source.
- Sex of the individual.
- Ancestry group.

To begin the Ancestry Estimation process it is necessary to gather all the elements from the database that contain data for at least the same cranial points as the Unknown, the individual being analyzed, to establish a direct comparison. First, the Unknown's points are filtered by identifying the those that have valid coordinates. A subsequent filtering is done to select only points present in many database entries as to maximize the number of shapes thus improving the overall accuracy. Finally, the resulting data is filtered for entries that have valid data for all those points and possess a valid ancestry and sex classification. If an entry doesn't have an ancestry or sex classification, having the respective data fields set to "Unknown", it can't be used for comparisons as so is discarded.

### **4.3 Generalized Procrustes Analysis**

To mitigate the effects of difference in scale, and rotation components between the sets of cranial points during the classification process all the shapes (the shapes from the database and the unknown shape) must be aligned. To this end the Generalized Procrustes Analysis algorithm, a statistical analysis method designed to superimpose a population of shapes, is applied. This algorithm works by performing the Procrustes Analysis (Kendall, 1989) to a population of shapes as opposed to only two. Procrustes Analysis superimposes two shapes by applying transformations to one as to remove the translational, rotational and uniform scaling components. This is accomplished by respectively translating the centroid to the origin, rotate one of the shapes so that their orientation matches and applying a uniform scale so that the root mean square distance to the origin is set to one. The difference between the resulting shapes can be then quantified by calculating the Procrustes Distance which is defined by the sum of square distances between corresponding points of both shapes. The Generalized Procrustes Analysis applies these principles to process a set of shapes by iteratively superimposing all the shapes to the mean shape calculated each iteration until convergence is achieved, determined by the difference between consecutive

Procrustes Distance between the reference and mean shape being below a predetermined threshold. If, however, convergence is not achieved, the mean shape is used in the next iteration as the reference shape and the Procrustes Analysis process restarts. The flowchart for this process can be seen in Figure 11.

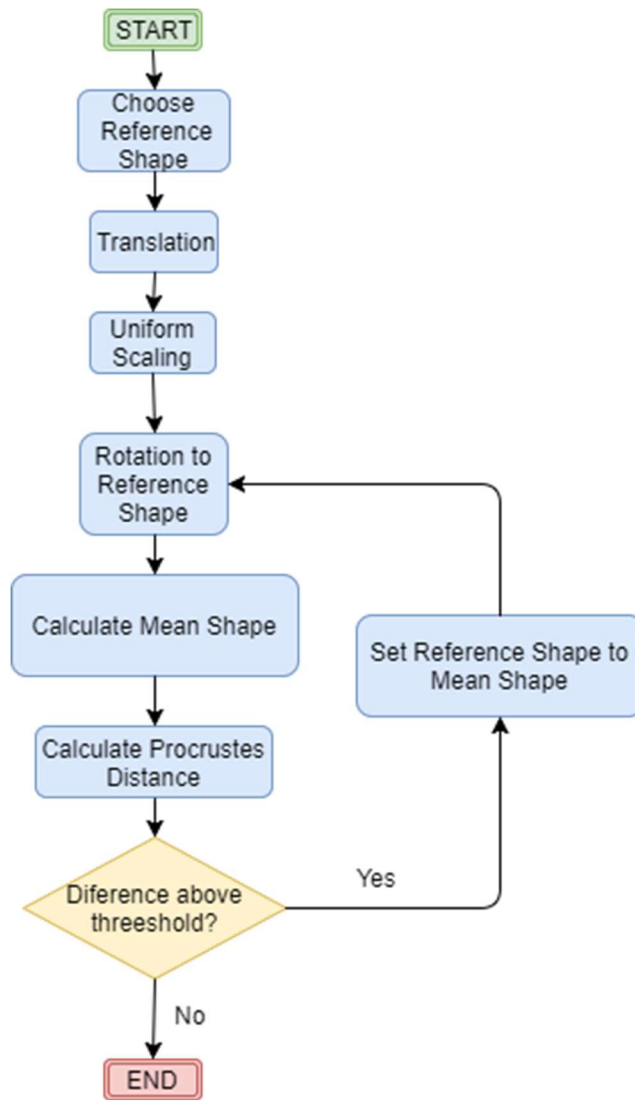


Figure 11 - Flowchart of the Generalized Procrustes Analysing algorithm used in the Ancestry Estimation process.

The following subsections detail each of the algorithms used to achieve convergence: translation, uniform scaling and rotation as well as the metric to evaluate it, the Mahalanobis distance.

### 4.3.1 Translation

All shapes are translated so that their centroid is translated to the origin of the coordinate system. To this effect the centroid is calculated by computing the average value of each coordinate component for all the points in that entry. The translation itself is applied by subtracting each point with the centroid calculated. This process is detailed in Equation 1 below.

$$\langle x_i, y_i, z_i \rangle \rightarrow \langle x_i - \bar{x}, y_i - \bar{y}, z_i - \bar{z} \rangle \quad \bar{x} = \frac{x_1 + \dots + x_k}{k}, \quad \bar{y} = \frac{y_1 + \dots + y_k}{k}, \quad \bar{z} = \frac{z_1 + \dots + z_k}{k} \quad (1)$$

Where  $i$  = point index,

$(x_i, y_i, z_i)$  = coordinates of the point being translated,

$(\bar{x}, \bar{y}, \bar{z})$  = averages of each of the coordinate component,

$k$  = total number of points.

### 4.3.2 Uniform Scaling

The shapes are then scaled so that the root mean squared distance of all the points to the origin is one. This is achieved by using the component average calculated during the translation process to obtain the scaling factor  $s$  through the square root of the sum of the squares of the difference of each coordinate and its respective mean divided by the number of points, show in Equation 2.

$$\langle x_i, y_i, z_i \rangle \rightarrow \langle x_i/s, y_i/s, z_i/s \rangle \quad s = \sqrt{\frac{(x_i - \bar{x})^2 + (y_i - \bar{y})^2 + (z_i - \bar{z})^2}{k}} \quad (2)$$

Where  $i$  = point index,

$(x_i, y_i, z_i)$  = coordinates of the point being translated,

$(\bar{x}, \bar{y}, \bar{z})$  = averages of each of the coordinate component,

$k$  = total number of points,

$s$  = scale factor.

### 4.3.3 Rotation to Reference

To remove the rotation component every shape must be rotated, using the rotation matrix  $R$ , so that it matches the rotation of the reference shape. The optimal 3 by 3 rotation matrix  $R$  is calculated as the solution to the Orthogonal Procrustes Problem (Everson, 1997). This problem can be solved by computing the Singular Value Decomposition (Schönemann, 1966) of the product of the matrix of the shape being rotated and the translated matrix of the reference shape. The rotation matrix is then defined by the product of the resulting  $V$  and  $U$  transposed matrices. All these steps are presented in Equation 3 below.

$$\begin{aligned}
C &= BA^T \\
C &= USV^T \text{ (Singular Value Decomposition of } C) \\
R &= VU^T
\end{aligned} \tag{3}$$

Where  $A$  = reference matrix,  
 $U$ ,  $S$  and  $V$  = resulting matrices from the Singular Value Decomposition,  
 $R$  = resulting rotation matrix.

### 4.3.4 Procrustes Distance

At the end of each iteration of the rotation to the current reference shape, the convergence is evaluated by firstly computing the mean shape calculating the Procrustes Distance, the sum of the squared distances between corresponding points, to the current reference shape. Equation 4 defines the Procrustes Distance.

$$d_i = \sqrt{(u_i - x_i)^2 + (v_i - y_i)^2 + (w_i - z_i)^2} \tag{4}$$

Where  $i$  = point index,  
 $d_i$  = Procrustes Distance,  
 $(x_i, y_i, z_i)$  and  $(u_i, v_i, w_i)$  = coordinates of  $i$ th point of both individuals.

The obtained value is then compared with the previous value and if the difference is below the threshold (considered empirically during optimization to be  $1 \times 10^{-5}$ ), the superposition is deemed as optimal and so the Generalized Procrustes Analysis is terminated. If on the other hand the difference is above the threshold it means the maximum convergence has not been achieved, the new reference shape is set to the mean shape calculated and another iteration of rotations to reference is performed and subsequently the convergence is tested in the same manner.

## 4.4 Classification

After all the database shapes, have been superimposed the next step is to compare them with the unknown individual to assign a classification. Initially, the Grand Mean matrix is determined by calculating the mean of all the previously superimposed shapes. The next step it is to fit the Unknown to the mean of all individuals. This alignment is done using the same process previously described: the unknown shape is modified to have the same scale, position and orientation as all the Grand Mean (translating centroid to origin, uniform scale so that root mean square distance of all the points is one and rotation with the Grand Mean matrix as a reference). Next all the database



and the Unknown shapes are mean corrected by subtracting the Grand Mean matrix. Finally, an average shape matrix is calculated for each group by computing the mean values of each point for all the shapes that are members of each ancestry group.

## 4.5 Mahalanobis Distance

The assignment of the Unknown to a group of shapes is done by calculating the Mahalanobis Distance between the mean shape of each group and the Unknown, being assigned to the group with the lowest value. The Mahalanobis Distance of a group, as shown in equation 5, is defined by the product of the transposed delta matrix, the inverse pooled covariance matrix and the delta matrix. The delta matrix is defined by the difference between the unknown shape matrix and the mean matrix of the group being analyzed.

$$D_i^2 = (x_{unknown} - \bar{x}_i)^T S_{pooled}^{-1} (x_{unknown} - \bar{x}_i) \quad (5)$$

Where  $i$  = point index,

$D_i^2$  = squared Mahalanobis Distance for the  $i$ th group,

$S_{pooled}^{-1}$  = inverse of the pooled covariance matrix

$g$  = number of groups

$X_i$  = matrix containing the shapes from the  $i$ th group.

The general formula for the Mahalanobis Distance uses a regular Covariance Matrix but, instead, a Pooled Covariance was used to further approximate the results given by the 3D-ID tool as the same type of matrix is used. The Pooled Covariance Matrix is calculated by first computing the Covariance Matrix for each shape group  $C_i$  and obtaining a weighted mean as shown in Equation 6.

$$S_{pooled} = \frac{1}{n} \sum_{i=0}^g n_i C_i \quad \text{where } C_i = \frac{X_i^T X_i}{n_i} \quad (6)$$

Where  $S_{pooled}$  = pooled covariance matrix,

$n$  = total number of shapes,

$n_i$  = number of shapes in the  $i$ th group,

$g$  = number of groups,

$X_i$  = matrix containing the shapes from the  $i$ th group.

## 4.6 Additional Metrics

Assigning a classification solely based on the lowest Mahalanobis Distance may not be sufficient because the low variability in the shapes caused by the superimposition process that may result in similar values between several classification groups. With this in mind additional metrics are used

to further support the classification process (van Vark and Howells, 1984). The metrics chosen were the ones originally used by the 3D-ID tool: the posterior probability and the “typicality” measure. The posterior probability, defined in Equation 7 indicates the relative closeness of the unknown shape to each group mean being that the ideal case would be high value for one group and zero for all the others, is calculated using the probability density function described in Equation 8.

$$\mathbf{Pr}(x_{unknown})_i = \frac{f(x_{unknown})_i}{\sum_{j=1}^g f(x_{unknown})_j} \quad (7)$$

$$f(x_{unknown})_i = \pi^{-v/2} \frac{\Gamma((n_f+1)/2)}{\Gamma((n_f-v+1)/2)} \left| \frac{(n_i+1)n_f}{n_i} S_{pooled} \right|^{-1/2} \left( 1 + \frac{n_i D_i^2}{n_f(n_i+1)} \right)^{-(n_f+1)/2} \quad (8)$$

Where  $i$  = point index,

Pr = posterior probability,

$f$  = probability density function,

$n_i$  = number of shapes in  $i$ th group,

$n_f$  = total number of shapes minus the number of groups,

$\Gamma$  = gamma function,

$D_i^2$  = Mahalanobis Distance for  $i$ th group.

The “typicality” measure helps gauge how likely the unknown shape came from a particular group despite the results for other groups. The “typicality” is calculated by finding the probability of the value defined in Equation 9 in a distribution  $F(v, n_f - v + 1)$ .

$$\frac{(n_f-v+1)n_i}{vn_f(n_i+1)} D_i^2 \quad (9)$$

Where  $i$  = point index,

$n_i$  = number of shapes in  $i$ th group,

$n_f$  = total number of shapes minus the number of groups,

$D_i^2$  = Mahalanobis Distance for  $i$ th group.



# 5 FRAGMENT RECONSTRUCTION

---

A significant number of the cranial remains recovered by the anthropologists are fragmented. These fragments vary wildly in number and size and can be damaged or even destroyed due to cadaver intrinsic and/or extrinsic factors. Reconstructing these fragments to take measurements present many difficulties. Setting the correct alignment for all the fragments can prove to be an extremely problematic task and is very susceptible to observer errors. When there are many fragments of a reduced size or when large portions are missing, the reconstruction cannot be done. Additionally, the reconstruction process itself is irreversible as the fragments are glued to each other which can be undesirable. Because of these reasons, the feature to be added to CraMs that was prioritized by the anthropologists was a semi-automated reconstruction system based on three-dimensional models from the scanned fragments. The idea is to allow to reconstruct the skull from the fragments to further process the reconstructed skull with the full range of tools available in CraMs Application.

## 5.1 Fragment Reconstruction Algorithms

Most computer assisted methods of reconstruction of archaeological fragments have three different stages: classification, reassembly and completion (Du et al., 2016). In the classification phase fragments are grouped based on similarities in curvature or texture color as to make sure that the fragments analyzed in the following stages belong to a single individual. During the fragment reassembly phase the fragments are subject to position and orientation changes to make them match, as close as possible, those of their original complete form. This can be done in one of two ways depending on the type of alignment: template-based or fracture-based. Finally, in the

completion phase, any incomplete regions caused by missing fragments, material subtracted during the fracturing process or erosion, of the produced skull are filled in with an estimated geometry. In the following subsections, these phases will be addressed in detail.

### **5.1.1 Fragment Classification**

To create an automated process for fragment reconstruction using individuals that originated from archeological sites it is imperative to establish a classification system to group them based on the individual they belong to. Most classification methods can be divided into two categories based on the classifying criteria: texture and geometric. Texture classification attempts to find similarities between the fragment's texture RGB values (Kampel, Sablatnig, 2000). Geometric Classification compare fragments by using the profile information which is the section of the fragment in the direction of the rotational axis (Sablatnig, Menard, Kropatsch, 1998). There are challenges associated with both classification methods: erosion causes a reduction of profile information and a great number of fragments may have textures that don't have significant differences.

### **5.1.2 Template-Based Reassembly**

The goal of template-based reassembly is to find partial correspondences between fragments and a pre-selected complete template model. The alignment of each of the fragments with the template can be done in several ways with the simplest being using an Iterative Closest Point (ICP) on both models (Yin, Wei, Li, and Manhein, 2011). This method is not very reliable as this algorithm is very susceptible to local minimums. Since the template model may differ from the fragmented model due to variability between individuals a direct comparison of geometry would not be suitable. This is the reason why many methods rely on keypoints. Keypoints are points in a 3D model with unique features and have the advantages of being scale and transformation invariant as well as providing better comparison performance as can be seen in Figure 12.

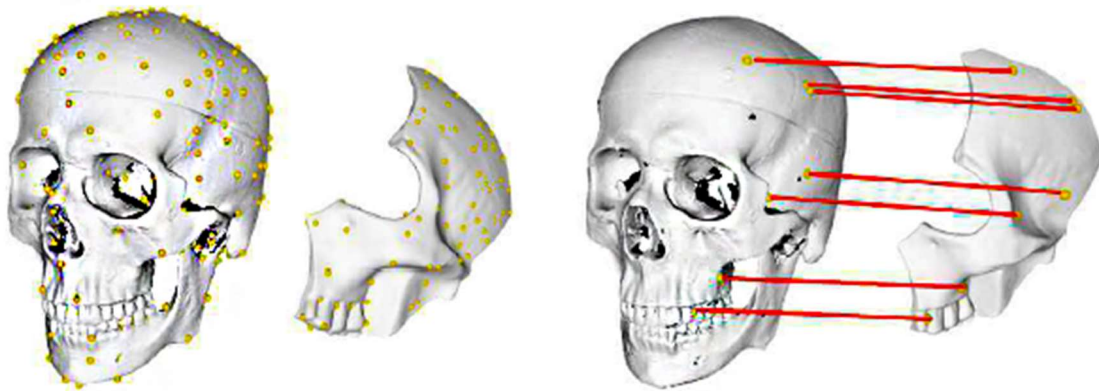


*Figure 12- Keypoint detection and matching for Template Based Reassembly. Taken from (Zhang, 2015).*

There are two main ways of obtaining the model keypoints: uniform sampling or calculation with a detector. With Uniform sampling the keypoints are spread out evenly throughout all the model. This method although simple is prone to error because the keypoints may not represent unique features. Alternatively, keypoint detection can be used. A possible algorithm used for keypoint selection is the Intrinsic Shape Signatures Algorithm (ISS) (Yu, 2009). ISS selects keypoints in regions of high curvature variance to ensure regions with very distinct geometry are used. For each keypoint a point descriptor is computed (a structure that characterize the point neighborhood with a goal of mitigating scale, orientation and noise). Among the most popular descriptors are Spin Images (Johnson & Hebert, 1999) that create 2D histograms of the accumulation of points when spinning around an axis, Point Feature Histogram (PFH) (Rusu, Blodow, & Beetz, 2009) which computes three values for each point pair based on the normal vectors and finally, the SHOT descriptor (Signatures of Histograms of Orientations) (Salti, Tombari, & Di Stefano, 2014) which creates a histogram of the cosine of normal vectors of the keypoint and each of the neighboring points in a sphere of customizable radius.

In real world situations, however some ambiguity between keypoints will inevitable produce a considerable number of false positive matches, namely because possible deformation of skull fragments due to deposition conditions. To mitigate this it is common to use some sort of consensus algorithm such as Random Sample Consensus (RANSAC) (Fischler & Bolles, 1981) to filter out the correspondences that diverge from the majority.

### 5.1.3 Fracture-Based Reassembly

Fracture-based reassembly analyses only a portion of the fragments: the fracture region, as opposed to the intact region, and finds geometric similarities between fragments to place them in the correct position and orientation so that the reassembly can be performed. Most fracture matching implementations use curvature to identify the fracture region. Multi-scale classification of the models is used to compute the feature curves (Pauly et al., 2003), the Minimum Spanning Tree (MST) of the identified high curvature points seen in Figure 13, which are then compared with the ones from other fragments to optimize their alignment. This solution presents several limitations as it was designed for small fragments where the biggest feature curves are the ones in the fracture region.

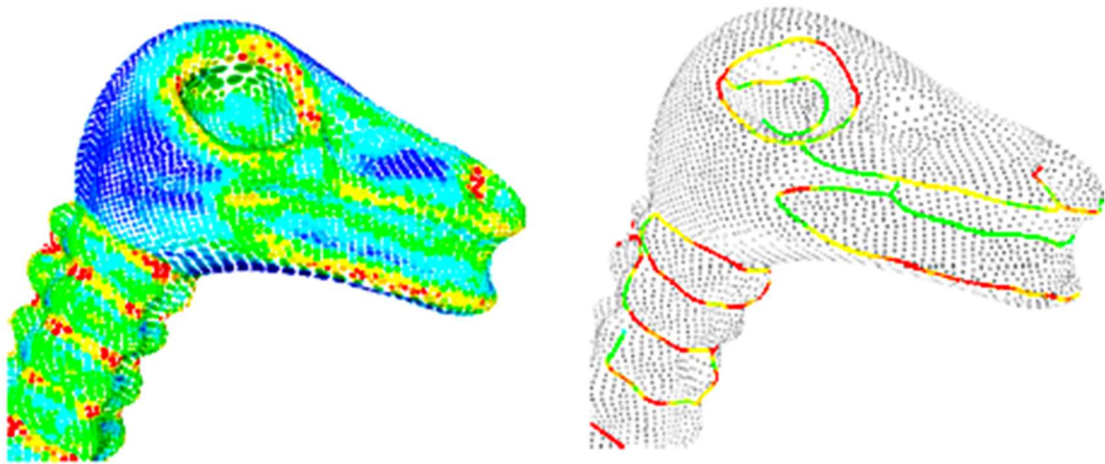


*Figure 13 – On the left curvature information, on the right the resulting MST. Taken from (Pauly et al, 2003).*

With of the two larger fragments from autopsies this is not the case as the feature lines would trigger false positives on intact regions or even the interior portions of the models and as such an alternative solution was put in place.

### 5.1.4 Hybrid Reassembly

The most effective approach however seems to be using the best of both worlds: applying a template based alignment to get a rough estimate of the fragments position relative to the complete template and improving the alignment by applying a fracture based alignment to make sure the fragments have the correct orientation and a flush against each other. An approach of this type (Zhang et al., 2015) was used as a starting point as it tackled the same problem, skull fragment reconstruction and showed good results with a completely automatic process. This method used both template based alignment (using ISS keypoint detector and SHOT descriptors) and a subsequent refinement using fracture region matching (using feature curves).

### 5.1.5 Skull Completion

Most of the individuals uncovered in archaeological sites are not complete and so the reconstruction will inevitably result in missing region in the newly formed skull. A possible solution to this problem is to fill these empty regions by exploiting symmetries in the human skull. The method proposed by (Yin et al., 2011) starts by determining the individual's symmetry plane and subsequently completes missing regions with data from the corresponding region relative to it. An alternative solution is to complete the missing regions using information from equivalent regions of a pre-selected template as can be seen in Figure 14.

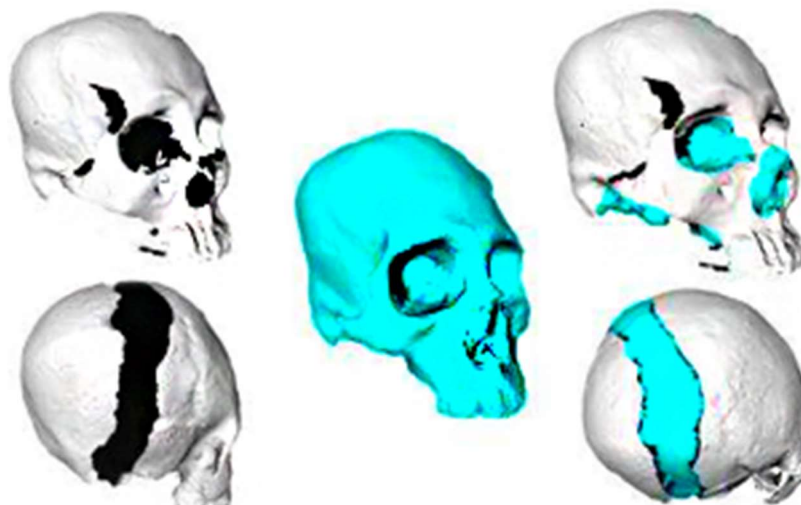


Figure 14– Template-based skull completion. Taken from (Wei, 2011).



## **5.2 Fragment Reconstruction within CraMs**

The primary goal of the CraMs fragment reconstruction method is to reconstruct individuals from the CEIXXI collection that were cut into two pieces to separate the calvarium from the rest of the skull during autopsy. Since the fragments were already grouped into corresponding pairs by the anthropologists the first reconstruction phase, the classification, does not apply and was not included into the solution design. Additionally, the last phase, the skull completion is not necessary because there are no missing fragments and a loss of material from the cutting process. The alignment process follow the hybrid approach, a rough pre-alignment using a template subsequently refined by a fracture-based alignment as this provided the upsides of both methods while only resulting in a negligible loss in performance. In the following sections the entire Fragment Reconstruction process, in all its iterations, is described detail as well as the reasoning supporting the choices made during its construction.

## **5.3 Rough Pre-Alignment**

### **5.3.1 Early Attempts with Automatic Template Alignment**

In the early stages of development, the solution for the rough pre-alignment used keypoint matching between each fragment and a template. This initial design used the ISS algorithm to calculate the keypoint for each of the models while creating descriptors for them using SHOT. Finally, the correspondences found by comparing descriptors are filtered the RANSAC algorithm.

The solutions in the literature that use this type of approach are built using the Point Cloud Library (PCL) as it provides a wide range of different tools for manipulation of 3D point clouds as well as implementations for most of algorithms for keypoints detection and descriptors referred in the previous sections including ISS, SHOT and RANSAC. For to this reason PCL was also integrated in CraMs to perform the background calculations while keeping VTK to handle the visualization and manipulation of the models.

However, despite several different variations of parameters on each of the algorithms in the alignment process, the obtained results were not satisfactory. Either the comparison was lenient and produced a very large number of incorrect correspondences, as seen in Figure 15, or was

stricter and it would allow limited variation with the models and thus produced very little correspondences. In both cases, causing the resulting alignment to be unusable. These errors were most likely due to the models used being double sided as opposed the thin-shelled models used in most solutions found in the literature. This caused the selection of keypoints on the inside geometry of the fragment's models and their subsequent incorrect matching with vertices on the template compromising the whole process. Due to these results, this approach was and a simpler semi-automatic solution had to be implemented in its place. PCL was also abandoned as a framework as its implementation of previously stated algorithms was no longer necessary.

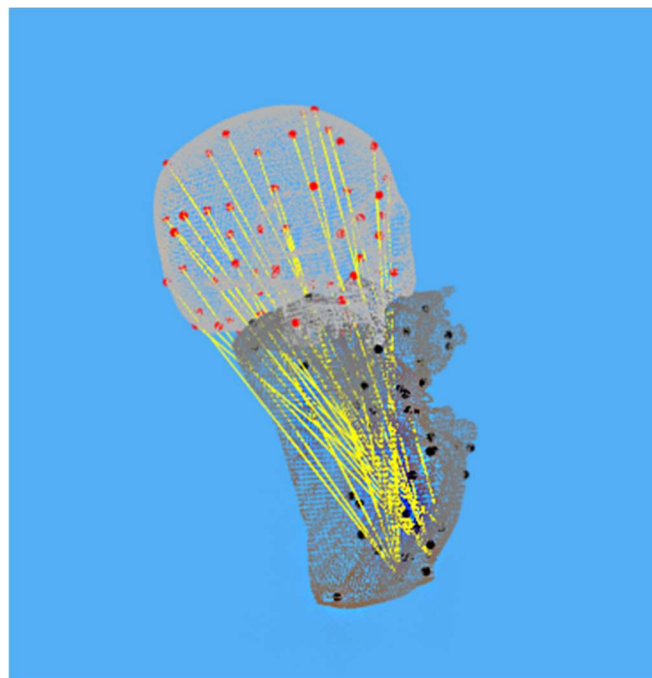


*Figure 15 – Problems with excessive false positive correspondences using Template-Based alignment.*

### **5.3.2 Semi-Automatic Alignment**

An initial system was created to align the fragments based on point correspondences between fragments. The user would be prompted to click on the corresponding vertices of the fracture in different fragments. The resulting transformation matrix was computed using the Rigid Body Transformation algorithm using these correspondences, with a proper result being produced if there are three or more, as input. This solution produced good results but it was quickly apparent that it was not viable for situations where there is a large number of small fragments as it would prove difficult and time consuming for a user to determine correspondences in a large and

ambiguous pool of fragments. The alignment method was repurposed to a system where the alignment would still be made through manual point correspondences between models but using a template model as basis instead. This solution has similar alignment result as the previous but it proves much more easy and efficient to use when it comes to smaller fragments as it is easier to identify known cranial points, especially for domain specialist. Both methods are represented in Figure 16.

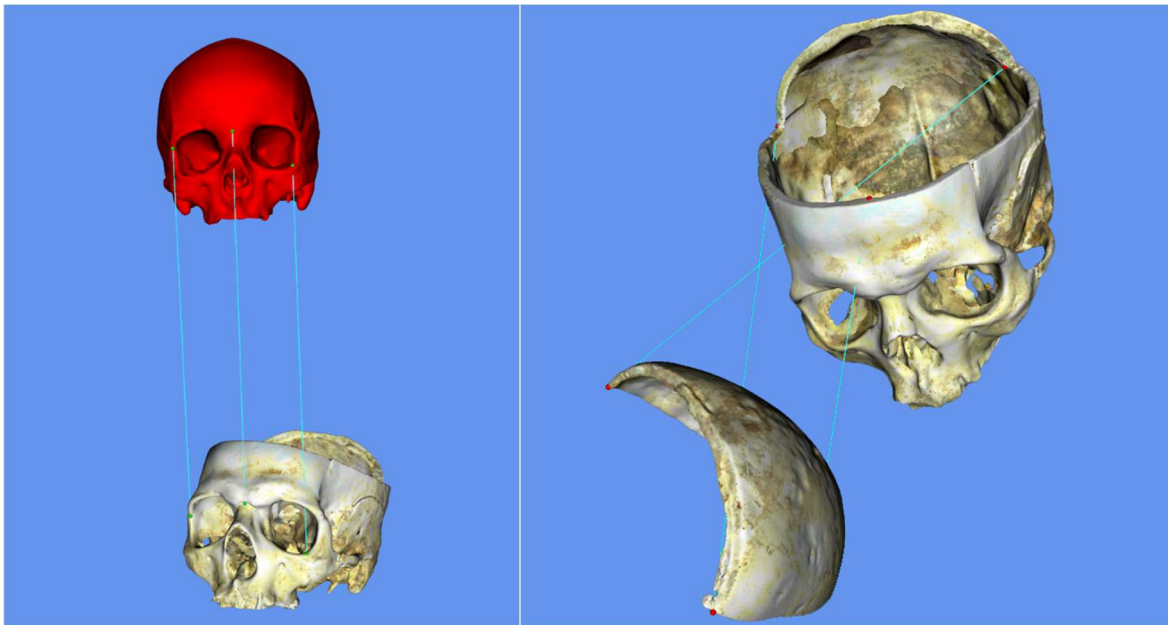


*Figure 16 - The pair-wise alignment processes with green spheres representing the points selected on each and the light blue lines joining corresponding points. On the left is the alignment between fragments and a template and on the right the alignment solely between fragments.*

## 5.4 Pair-wise Refinement

With fragments now pre-aligned the next step is to refine their alignment to assure neighboring fragments perfectly match each other. As discussed in section 5.1.3 most solutions accomplish this by using curvature information to define the fractures of each fragment and so a similar approach was used in CraMs. The implemented solution relies on the fact that fracture is composed of regions with the same orientation and low curvature variation. The whole fracture could be defined using a handful of points on the fractures, called seed points, and a region growing mechanism using

those conditions. Subsequently the transformation matrix can be derived from these fractures producing a more precise alignment between fragment pairs thus improving the reconstruction's overall accuracy.

There are some assumptions that can be made when calculating seed points between neighboring points. Firstly, since the fractures by definition are on the fragment's edges facing each other, we can safely say that on equivalent regions the closest pairs of vertices are in their respective fractures. Secondly, we can be sure that the orientation of point pairs in the fragment is inverted within a margin to account for different orientations and fracture erosion.

Now that these conditions have been established to filter the seed points the simplest solution is to filter every pair of points. This presents a problem since a fragment model could have more than a million vertices resulting in very time consuming brute force algorithm if pairwise comparison were performed on the whole datasets. A different approach, computationally less costly, by restricting the points to those in the region in between fragments. To define this region some points are calculated, called probe points, that are then used as reference when calculating seed points. Finally, the computed regions are used as input for an ICP algorithm to align them, producing a transformation matrix which can then be applied to the whole fragments. These four steps in this process, from obtaining the seed points to computing the resulting transformation matrix, can be seen in Figure 17.



Figure 17 - Workflow for the Pair-wise Alignment refinement.

### 5.4.1 Probe Point Determination

The first step is to slightly separate fragments. This is done to remove any intersections between the fragments to add robustness in case of a poor pre-alignment. Since the relative orientation between fragments must be preserved the separation vector must correspond to the vector between them. To approximate this, the separation vector is computed using the fragment's

centers of mass obtained using the VTK tool *vtkCenterOfMass*. The length of the separation vector is set to 50% of the original vector between the centers of mass considering that clipping from the template alignment is very mild

The next step is to find the points in between the fragments, the probe points, that will serve as the basis for the calculation of the seed points in the fracture region. First, the new centers of mass are calculated, as they change after the initial separation, and with those it is possible to define an intermediary plane between the fragments defined as the plane perpendicular to the vector formed by the two centers of mass and centered on the midpoint between them. Since the overwhelming majority of the vertices belonging to the fracture region are on regions of the model further away from its center of mass, the probe points are distributed in a rectangle formation. This rectangle is calculated from the intersection of a cuboid with the same dimension's average of the two bounding boxes and the intermediary plane obtained previously. The number of probe points, interpolated in the resulting rectangle, can be set by the user to any number larger than four. The default value being sixteen as seen in Figure 18.

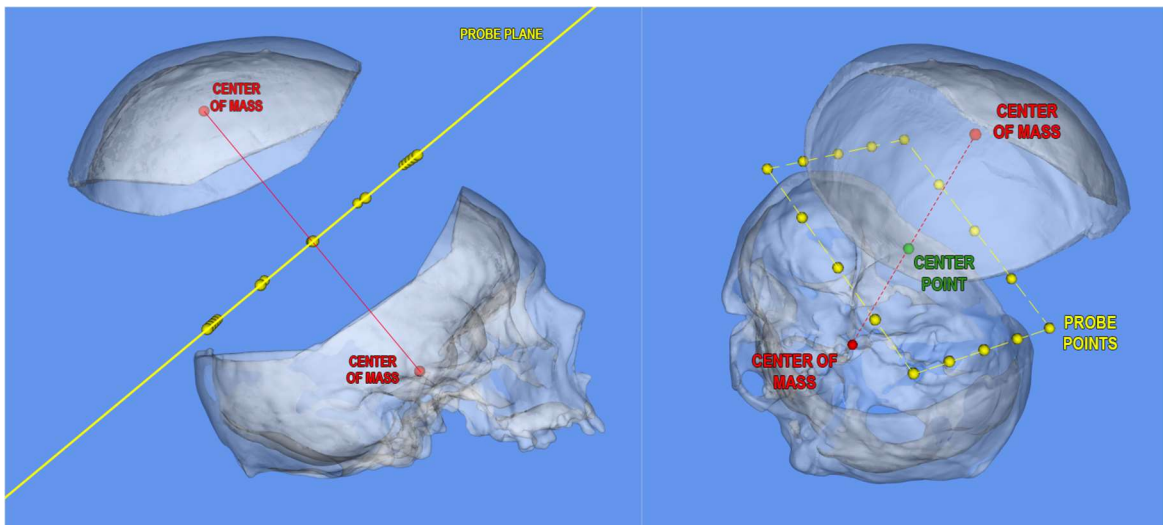


*Figure 18- On the left is a side view of two neighboring fragments with their centers of mass represented by red spheres, the middle plane perpendicular to line between them in orange and the probe points in yellow. On the right is a top down view of the probe point represented as yellow sphere organized as a rectangle with its center as a green sphere.*

## 5.4.2 Seed Point Calculation

Now after determining the probe points have been determined it is possible to calculate the seed point of the fracture region for each fragment. Initially, a group of candidate points for each probe point are obtained by computing the 150 closest vertices to each of the fragments using a K-d Tree.

Then from both candidate groups the same number of probe point a seed point is selected, for each of the fragments, based on two criteria: minimal distance and closest to symmetrical normal vectors as can be seen in Figure 19. The minimal distance criteria have the purpose to select only points from the border of fragments thus removing unwanted points from either side of the intact region. The normal symmetry criteria find the points whose normal vectors are closest to the inverse of one another filtering out unwanted regions from either the sides of the interior of the model. Additionally, a restriction on the low point curvature is also applied to ensure that the seed point selected is not on a sharp edge as not to disturb the fracture region expansion explained below.

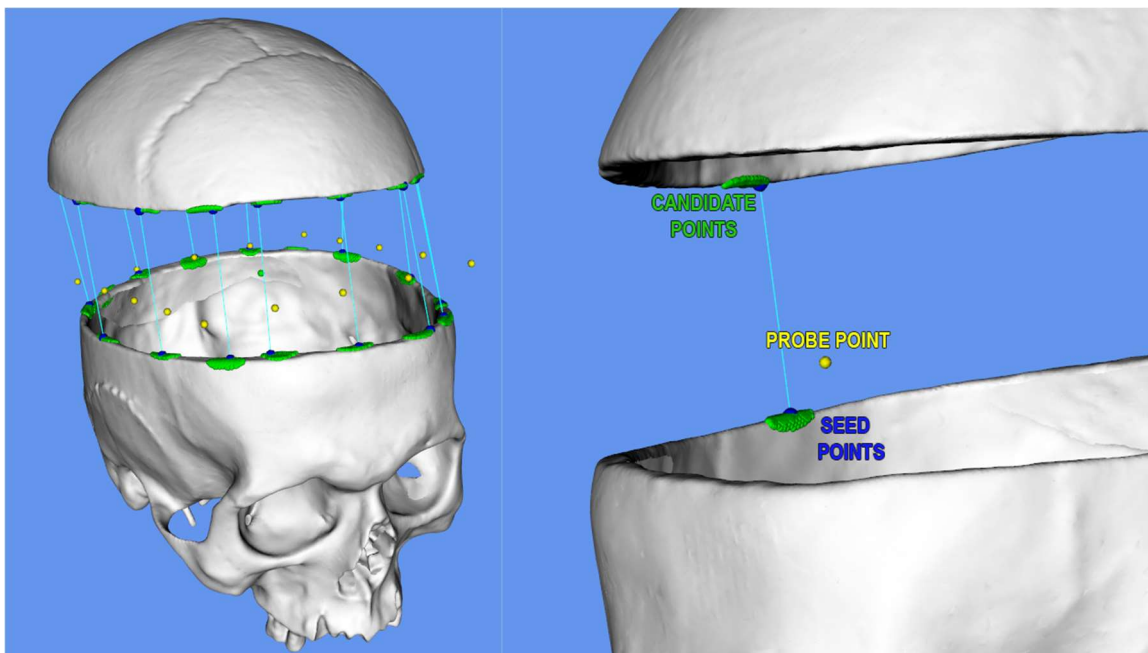


*Figure 19 - View of the 150 candidate vertices for each probe point on each fragment (green spheres) with the selected seed points (blue spheres) and the corresponding seed points joined by a light blue line.*

### 5.4.3 Fracture Region Expansion

The final step in this process is to compute the points in the fracture region using the seed points. A queue of points is created, starting with the seed points, and each connected point is iteratively tested for curvature. If a point has a curvature similar to that of the seed point it corresponds to the fracture region and is added to the queue to be processed. Otherwise if the point has a high absolute curvature value so it then corresponds to the edge of the fracture region and so it is not inserted into the queue stopping the search in that direction. The curvature threshold must be kept low as not to “spill” the fracture region onto the sides since a single point could compromise the whole region. The inserted points in the queue are tested for duplication to avoid the expansion of the same points multiple times and a subsequent cleanup of these overlapping regions. The resulting fracture regions can be seen in Figure 20.

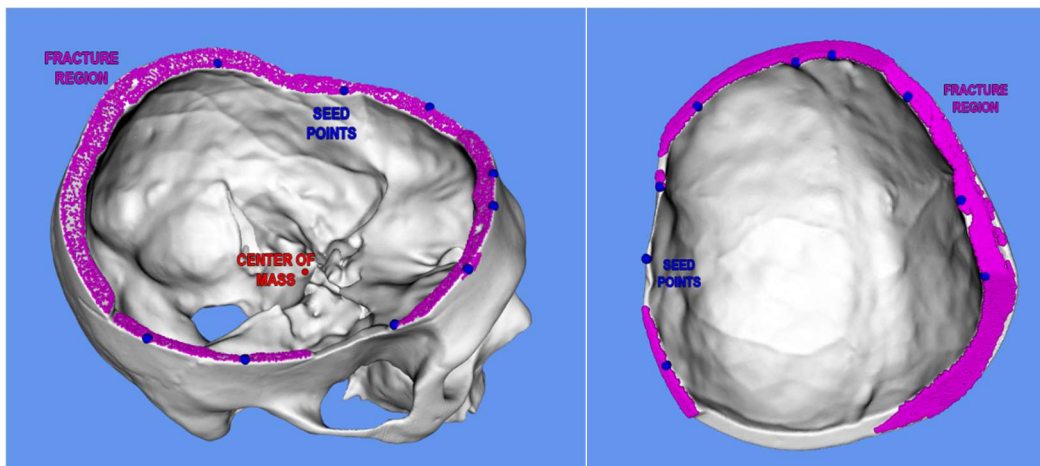
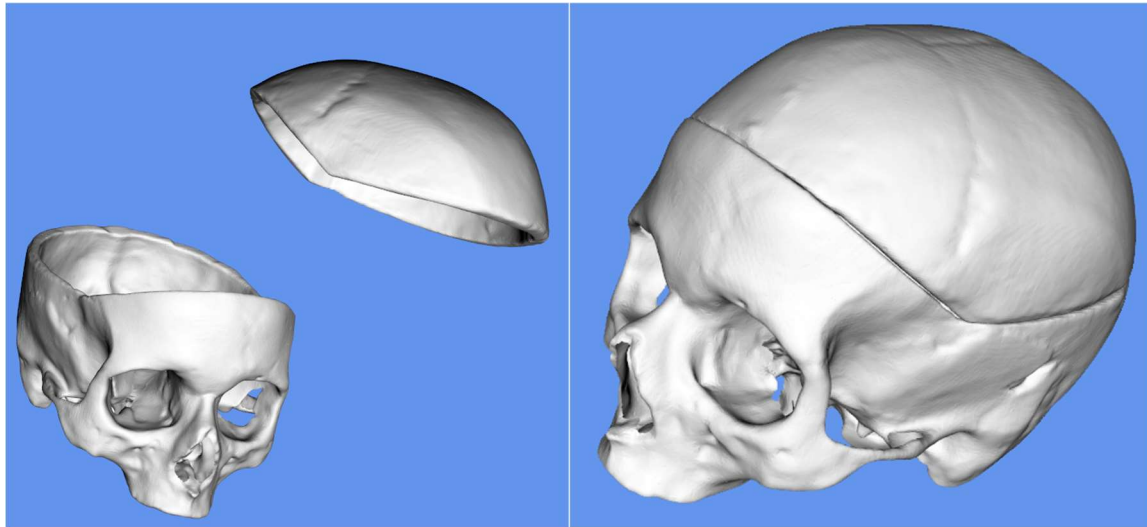


Figure 20 - Expanded fracture region in purple generated from the seed points seen as blue spheres. The red sphere represents the center of mass of the fragment.

### 5.4.4 Computing and Applying Transformation

To complete the reconstruction the Iterative Closest Point algorithm (ICP) is applied to the resulting fracture regions from each of the fragments. This algorithm superimposed both fragment regions, minimizing the distance between for a maximum of 150 iterations, a number that was determined empirically during testing to produce proper alignment. The resulting matrix is then applied to the fragment model whose fracture region was used as a source in the ICP process. The resulting model and the original fragments are shown in Figure 21.





*Figure 21 – On the left the fragments before the reconstruction and on the right the resulting reconstructed skull.*

#### **5.4.5 Semi-Automatic Region Expansion**

Since the CraMs application's target users are professionals a semi-automatic solution was required as an alternative to correct eventual misalignments. This solution used the same principles of fracture region growing detailed in the previous sections but with manual user defined seed points. The semi-automatic solution for fragment reconstruction works on a single fragment at a time. The user chooses a seed point by selecting the point on the model. The fracture region is then calculated as in the automatic solution, finding connected points with low curvature. The user can mark as many seed points as he/she wants, until the fracture region is deemed to be covering the entire fracture and so ready to be reconstructed.





# 6 RESULTS

---

This chapter presents the results obtained for both the Ancestry Estimation and the fragment reconstruction processes. In the first section the Ancestry Estimation algorithm is applied to nineteen individuals with varying numbers of point data defined by the experts. The classification results are compared to the classification assigned by the anthropologists using the methodology defined by (Hefner, 2009) as well as the classification produced by the 3D-ID in order to validate the solution. The second section presents the reconstruction of nine fragmented individuals from autopsies reconstructed with the system developed in CraMs. To assess the validity of this solution the results are compared with the physical reconstruction using a craniometric measurement the Basion-Bregma Height, a visual evaluation performed by the anthropologists and the average distance between fracture distances

## 6.1 Ancestry Estimation

To evaluate the accuracy of the Ancestry Estimation solution implemented we must compare the classification results obtained with those assigned by the anthropologists for each set of cranial remains. The effectiveness of the classification process increases with the more points used because the differences between groups are more defined. Due to this fact, the PAV 09 collection, a collection of remains from African slaves, was used as these had 19 individuals with a large amount of points marked by the anthropologists while other collections would have had to be used with automatic points generated by CraMs. These points are subsequently filtered during the Ancestry Estimation process as described in section 4.2, selecting those that are common in the

database resulting in even fewer points being used. Table 2 shows which points were used in the Ancestry Estimation process for every individual marked by the anthropologists.

*Table 2 – Points used to test the Ancestry Estimation process for each individual. The abbreviations of the point names follow the rules described in Annex 1.*

<b>ID</b>	<b>Points</b>	<b>Count</b>
PAVd09_121	B, N, Pr, Right Ekm, Left Ekm, L, Left Inferior Orbit, Left Superior Orbit, Right Ek, Left Ek	11
PAVd09_125	B, Ba, Right Zy, Left Zy, G, N, Pr, Right Ekm, Left Ekm, L, O, Left Inferior Orbit, Left Superior Orbit, Right Ek, Left Ek	15
PAVd09_138	B, Ba, G, N, Pr, Right Ekm, Left Ekm, L, O, Right D, Left D	11
PAVd09_139	B, G, N, Pr, Right Ekm, Left Ekm, L, Right D, Left D	11
PAVd09_157	B, G, N, Pr, Right Ekm, Left Ekm, L, Right D, Left D	9
PAVd09_165	B, Ba, Right Zy, Left Zy, G, N, Pr, Right Ekm, Left Ekm, L, O, Left Inferior Orbit, Right Superior Orbit, Right Ek, Left Ek	15
PAVd09_166	B, Ba, G, N, Pr, Right Ekm, Left Ekm, L, O, Right D, Left D	11
PAVd09_167	B, Ba, Right Zy, Left Zy, G, N, Pr, Right Ekm, Left Ekm, L, O, Right D, Left D	13
PAVd09_175	B, G, N, Pr, Right Ekm, Left Ekm, L	7
PAVd09_177	B, Right Zy, Left Zy, G, N, Pr, Right Ekm, Left Ekm, L, O	10
PAVd09_178	B, Ba, G, N, L, O	6
PAVd09_181	B, G, N, Pr, Right Ekm, Left Ekm, L, Right D, Left D	9
PAVd09_182	B, Ba, Right Zy, Left Zy, G, N, Pr, L, O, Right D, Left D	13
PAVd09_193	B, Ba, Right Zy, Left Zy, G, N, O	7
PAVd09_196	B, Ba, G, N, L, O	6
PAVd09_1110	B, Ba, Right Zy, Left Zy, G, N, Pr, L, O	6
PAVd09_1133	B, Ba, Right Zy, Left Zy, G, Right Ekm, Left Ekm, O	8
PAVd09_1163	B, Ba, G, N, Pr, Right Ekm, Left Ekm, L, O, Right D, Left D	11
PAVd09_1169	B, Ba, G, N, Pr, Right Ekm, Left Ekm, L, O, Right D, Left D	11

The individuals along with their point marking files were loaded into CraMs to generate its classification. Subsequently the point coordinates were manually inputted into 3D-ID to obtain its classification results for comparison. The results for each of the individuals tested using CraMs and

3D-ID can be seen in Table 3. From the results of the two solutions the four output values were collected:

- Classification: the ancestry group assigned.
- D2: the squared Mahalanobis Distance between the individual and said group.
- P: the posterior probability.
- T: the “typicality” measure.

*Table 3 - Results of Ancestry Estimation applied to the individuals with points marked by the anthropologists using CraMs and 3D-ID marked with green when correctly identified and red when otherwise.*

ID	CraMs				3D-ID			
	Classification	D2	P	T	Classification	D2	P	T
PAVd09_I21	African F	32.94	0.92	0.67	African F	42.29	0.96	0.27
PAVd09_I25	African F	90.07	0.69	1.27	African M	92.02	0.66	0.01
PAVd09_I38	African M	21.16	0.47	0.46	African M	22.37	0.59	0.90
PAVd09_I39	African American F	3032	0	0	African American M	1291	0	0
PAVd09_I57	African F	20.90	0.08	0.53	Mesoamerican F	25.23	0.39	0.44
PAVd09_I65	African F	69.95	0.38	0.99	African M	77.81	0.98	0.03
PAVd09_I66	African F	33.83	0.28	0.69	African F	40.38	0.52	0.33
PAVd09_I67	CircumCaribbean M	25.52	0.09	0.49	African M	28.3	0.61	0.92
PAVd09_I75	South American M	19.77	0.23	0.59	South American F	18.59	0.79	0.38
PAVd09_I77	CircumCaribbean M	22.86	0.05	0.59	Mesoamerican M	22.62	0.64	0.61
PAVd09_I78	CircumCaribbean F	9.72	0.09	0.42	African American F	9.01	0.22	0.64
PAVd09_I81	African M	8.89	0.23	0.24	African M	9.16	0.42	0.99
PAVd09_I82	MesoAmerican F	26.75	0.31	0.45	MesoAmerican F	30.43	0.25	0.88
PAVd09_I93	African F	11.27	0.11	0.43	African F	10.60	0.37	0.85
PAVd09_I96	African F	12.91	0.06	0.58	African American F	11.60	0.23	0.41
PAVd09_I110	CircumCaribbean F	13.74	0.09	0.59	East Asian M	9.05	0.65	0.72
PAVd09_I133	African F	17.14	0.11	0.45	African American F	15.53	0.60	0.78
PAVd09_I163	African M	12.77	0.12	0.43	African M	15.89	0.52	0.72

PAVd09_I169	African M	29.23	0.11	0.64	African M	28.08	0.71	0.72
-------------	-----------	-------	------	------	-----------	-------	------	------

The Ancestry Estimation solution developed in CraMs correctly classified the individuals as African in 13 out of the 19 cases or 68.4% with the remaining individuals being classified as South and Central American. This contrasts with the results obtained using 3D-ID that produced a correct classification in 14 individuals or 73.7%. This difference can be attributed to the use of a significantly larger dataset with 3D-ID compared to the CraMs solution. Additionally, we can confirm that a larger number of points contributes greatly to the success rate of the Ancestry Estimation within CraMs, as expected, with 9 of the total 19 individuals used less than 10 points and had a success rate of 55.6% while the remaining 10 individuals used between more than 10 points and had a success rate of 70%.

## 6.2 Fragment Reconstruction

The Fragment Reconstruction solution implemented in CraMs was applied to all the fragmented models available, eight autopsied individuals with their calvarium removed, from the CEIXXI collection to evaluate its effectiveness. Initially the plan was to evaluate the reconstruction by comparing the resulting 3D model with the one obtained from acquisition of the fragments reconstructed manually by the anthropologists. During testing, however, it was concluded that due to the very high sensitivity of the 3D Scanner, in the order of microns, obtain accurate readings of the reconstructed model was impossible without permanently fusing the fragments. Since direct comparison was not feasible two alternative metrics had to be devised: comparing craniometric measurements between the physical and digital reconstruction and a visual evaluation done by the anthropologists.

Getting accurate craniometric measurements from a manually reconstructed skull poses difficulties as the direct comparison with measurement inaccuracies or even missing landmark points. Due to this only one measurement could be reliably obtained, the Basion-Bregma Height (BBH). The measurement was obtained by the anthropologists on the physically reconstructed specimens to be subsequently compared to the one calculated on the digital reconstructed using CraMs. Table 4 show the values obtained from both reconstructions, for each of the autopsied individuals.

Table 4– Results of the Reconstruction comparison between the physical reconstruction and the one done using CraMs using Basion-Bregma Height measurements.

<i>ID</i>	<b>Physical BBH (mm)</b>	<b>CraMs BBH (mm)</b>	<b>ΔBBH</b>	<b>Observations</b>
CEIXXI_CRN_025_F	127	127.29	0.29	
CEIXXI_CRN_030_M	135	133.20	1.8	
CEIXXI_CRN_074_M	-----	-----	-----	Impossible to measure on physical specimen.
CEIXXI_CRN_083_M	140	141.62	1.62	
CEIXXI_CRN_107_F	131	130.13	0.87	
CEIXXI_CRN_114_F	145	144.49	0.51	Sutures on model not clear. Unsure on the position of the Bregma.
CEIXXI_CRN_141_M	140	141.22	1.22	
CEIXXI_CRN_146_F	137	135.80	1.2	
CEIXXI_CRN_165_M	140	139.39	0.61	

The results indicated that the digital reconstruction was very similar to its physical counterpart with the difference between Basion-Bregma Heights not exceeding 2mm and with a 1.02mm average. To further validate this solution the technical error of measurements (TEM), defined by (Perini, Oliveira, Ornellas, & Oliveira, 2005), must be calculated. The TEM represents the standard deviation between repeated measurements and is a common way of expression error margin having been used in (Andrade, 2016; Neves, 2014; Santos, 2013) for validation. It is defined by equation 10 and equation 11.

$$Absolute\ TEM = \sqrt{\frac{\sum d_i^2}{2n}} \quad (10)$$

$$Relative\ TEM = \frac{Absolute\ TEM}{VAV} * 100 \quad (11)$$

Where  $\sum d_i^2$  = summation of measure deviations squared

$n$  = number to total measures

$i$  = index of the measure

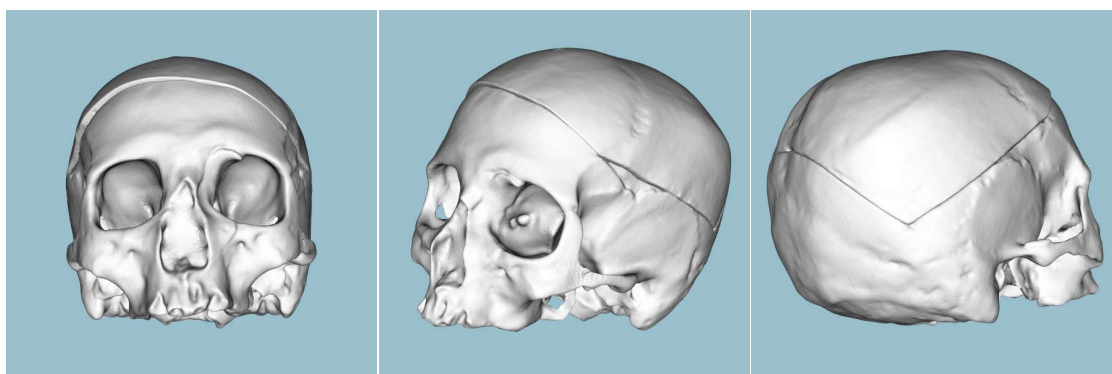
$VAV$  = variable average value (arithmetic mean between the measurements).

The TEM is expressed in percentage and typically a value above 10% means the measure is unacceptable. Applying the TEM formula to the results presented in Table 3 results in a TEM value of 0.59% being well below the threshold.

To complement this metric a method was devised using grading based on visual inspection. Visual inspection was done by the experts using a scale between 1 and 5, with 1 being a unacceptable reconstruction of the fragments and a 5 being a perfect alignment. The anthropologists were also asked to complement this evaluation with observations about the digital and physical reconstruction. Additionally, the average distance between the points in the fracture regions of the fragments (AFD) after the ICP transformation is applied was also calculated.

Below the results of the digital reconstructions applied to the 9 individuals is presented with three images of the resulting model, the evaluation done by the anthropologists and the average distance between the fracture regions calculated. The classification and AFD results for all the individuals are also shown in Table 5.

**ID:** CEIXXI\_CRN\_025\_F



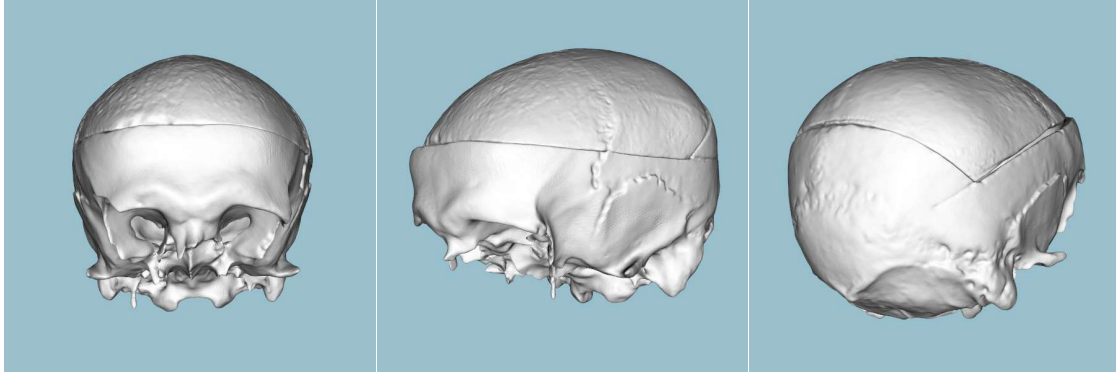
**Physical Reconstruction Observations:** Doesn't fit well due to Post-Mortem deformation.

**Digital Reconstruction Observations:** Is in accordance with the real individual.

**Classification:** 5

**Average Fracture Distance:** 1.09 mm

**ID:** CEIXXI\_CRN\_030\_M



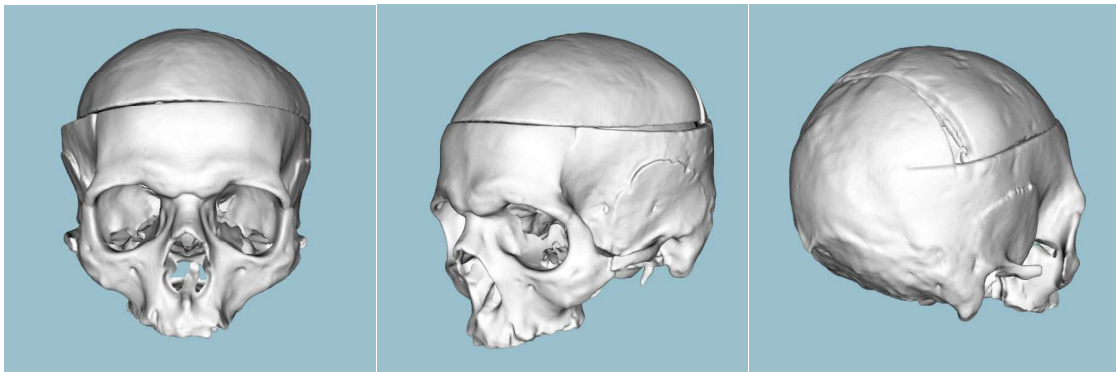
**Physical Reconstruction Observations:** Doesn't fit well due to Post-Mortem deformation.

**Digital Reconstruction Observations:** Is in accordance with the real individual.

**Classification:** 5

**Average Fracture Distance:** 2.12 mm

**ID:** CEIXXI\_CRN\_074\_M



**Physical Reconstruction Observations:** Fits well with no Post-Mortem deformation.

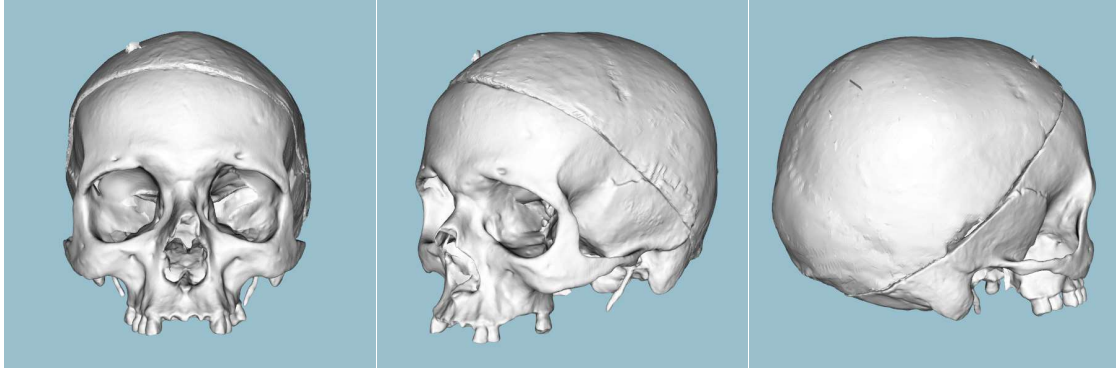
**Digital Reconstruction Observations:** Doesn't fit well and appear to have Post-Mortem deformation.

**Classification:** 1

**Average Fracture Distance:** 15.36 mm



ID: CEIXXI\_CRN\_083\_M



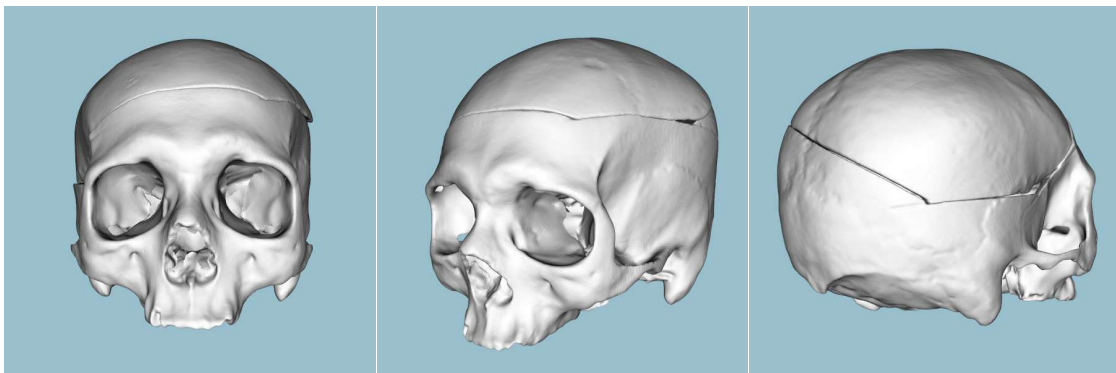
**Physical Reconstruction Observations:** Fits well. Missing portion of Occipital bone. Isn't stable due to the nature of the autopsy incision.

**Digital Reconstruction Observations:** Is in accordance with the real individual.

**Classification:** 5

**Average Fracture Distance:** 0.95 mm

ID: CEIXXI\_CRN\_107\_F



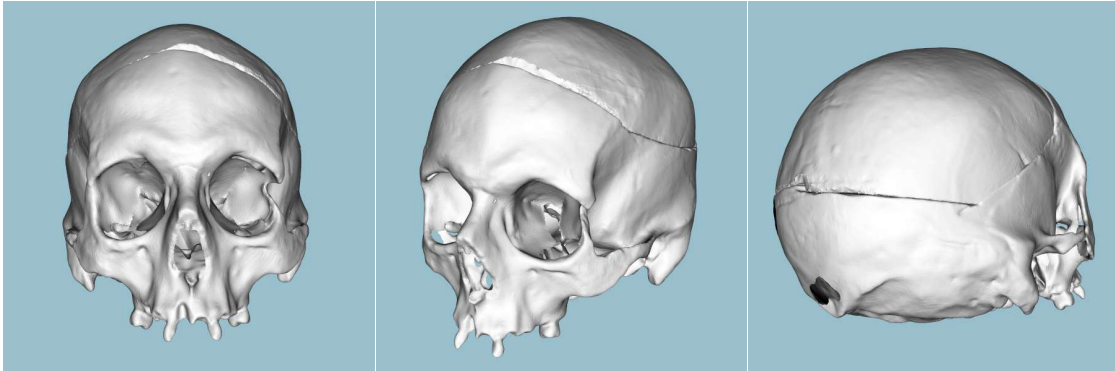
**Physical Reconstruction Observations:** As low Post-Mortem deformation. Missing left parietal bone and right temporal bone.

**Digital Reconstruction Observations:** Is in accordance with the real individual.

**Classification:** 5

**Average Fracture Distance:** 0.76 mm

**ID:** CEIXXI\_CRN\_114\_F



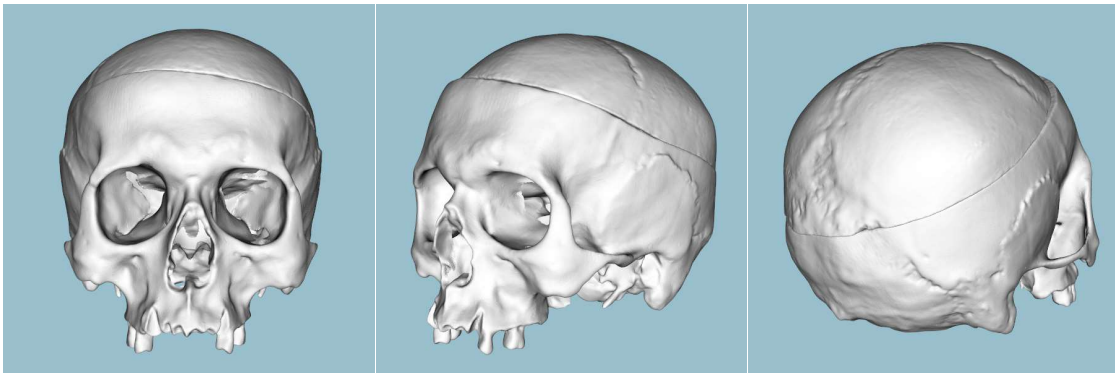
**Physical Reconstruction Observations:** Fits perfectly with no Post-Mortem deformation.

**Digital Reconstruction Observations:** Is in accordance with the real individual.

**Classification:** 5

**Average Fracture Distance:** 0.63 mm

**ID:** CEIXXI\_CRN\_141\_M



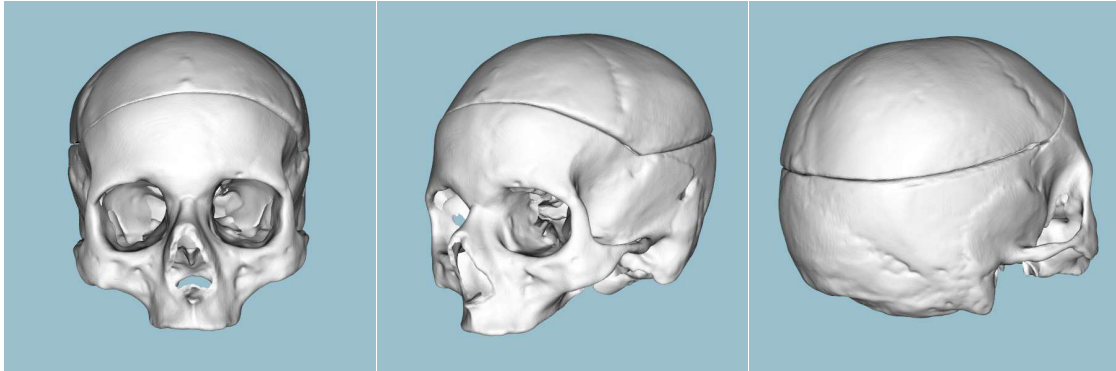
**Physical Reconstruction Observations:** Fits well. Missing bone in the Frontal bone.

**Digital Reconstruction Observations:** Scalp should be shifted towards the orbits.

**Classification:** 3

**Average Fracture Distance:** 1.57 mm

**ID:** CEIXXI\_CRN\_146\_F



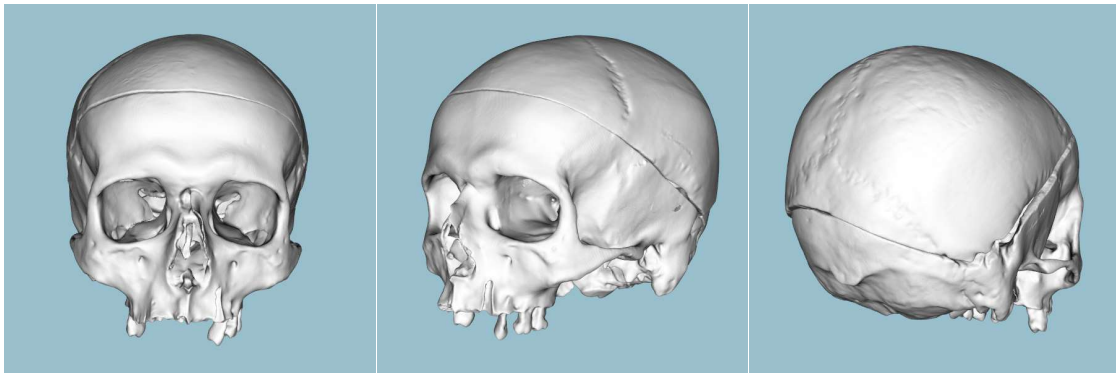
**Physical Reconstruction Observations:** Fits well. Reconstruction is stable.

**Digital Reconstruction Observations:** Doesn't fit completely.

**Classification:** 4

**Average Fracture Distance:** 0.63 mm

**ID:** CEIXXI\_CRN\_165\_M



**Physical Reconstruction Observations:** Fits well. Missing bone in the right Temporal bone.

**Digital Reconstruction Observations:** Is in accordance with the real individual.

**Classification:** 5

**Average Fracture Distance:** 3.41 mm

*Table 5 – Results of visual classification done by the antropologists and average fracture distance of the reconstruction done using CraMs.*

<b>ID</b>	<b>Classification</b>	<b>Average Fracture Distance(mm)</b>
CEIXXI_CRN_025_F	5	1.09
CEIXXI_CRN_030_M	5	2.12
CEIXXI_CRN_074_M	1	15.36
CEIXXI_CRN_083_M	5	0.95
CEIXXI_CRN_107_F	5	0.75
CEIXXI_CRN_114_F	5	0.63
CEIXXI_CRN_141_M	3	1.53
CEIXXI_CRN_146_F	4	0.63
CEIXXI_CRN_165_M	5	3.41

The evaluation of the reconstructions by the anthropologists is very positive as can be seen in Figure 22. Two thirds of the reconstructions were assessed by the experts as perfect, a “5”, and produced similar results to the physical reconstruction. Two individuals, number 146 and 141, were evaluated with “4” and “3” respectively. These reconstructions are mostly correct and only require a slight shift in position and orientation.

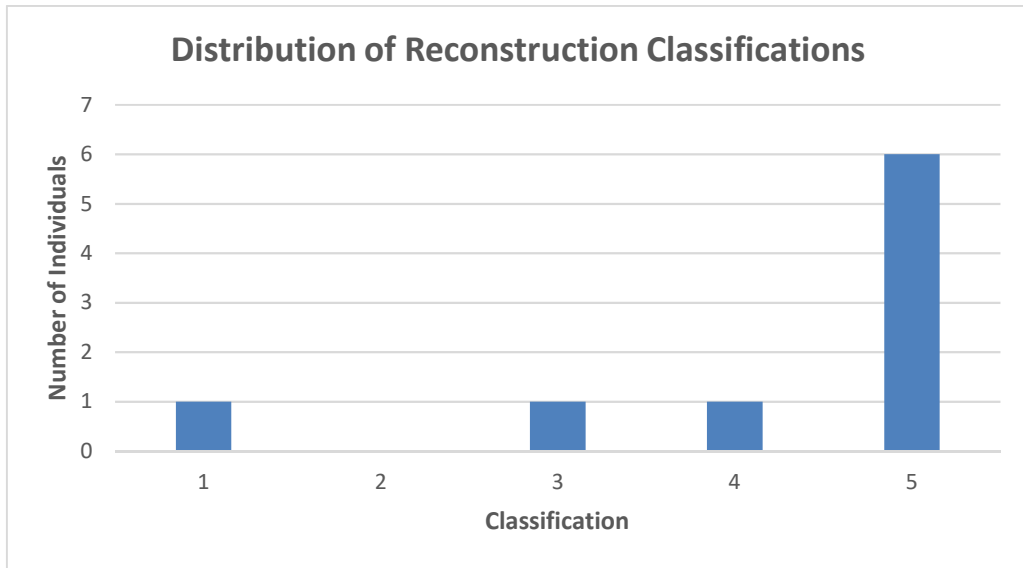


*Figure 22 – Representation of the distribution of reconstructions by classification given by the anthropologists.*

One individual, number 74, was completely misaligned by the experts (evaluated with a one). This is caused by the limitations in the methods used to calculate the fracture region. Since the calculation of the search points described in section 5.4 follows the abstraction of a rectangle projected to a plane between the fragments points in the fractures perpendicular to this plane are not correctly detected as shown in Figure 23. The ICP alignment is then applied to fracture regions that are potentially very different thus causing the misalignment.

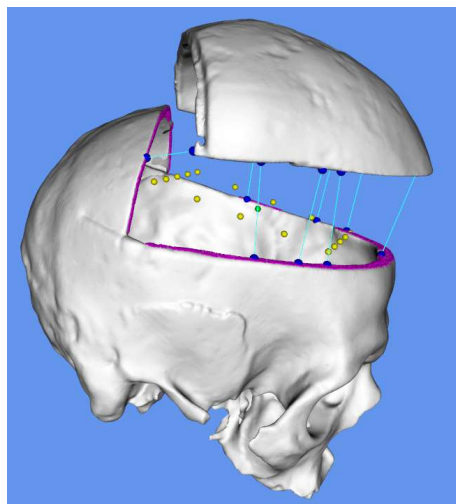


*Figure 23 - Problems detecting the fracture region in calvarium areas perpendicular to the probe planes on individual 74.*

The average fracture distance is the distance calculated between the fracture regions. This is done by averaging the distance obtained by iterating through every point in one of the fragment's model and closest point in the opposing fragment using K-D trees. This value can be correlated with the success of the reconstruction to only some degree, clearly differentiating very poor reconstructions, those evaluated with "1", but not providing a large enough distinction for classifications between "3" and "5", as can be seen in Figure 24.

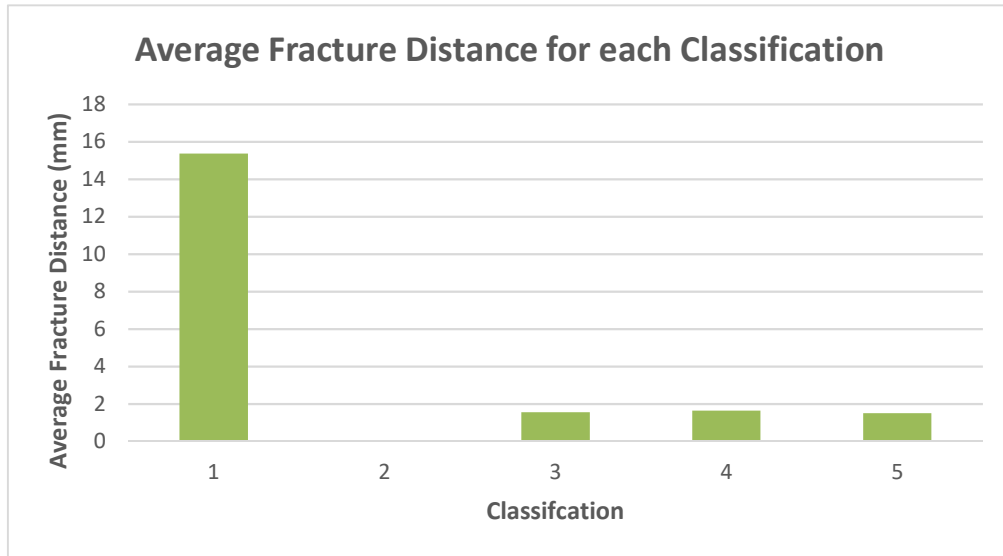


Figure 24 - Average Fracture Distance of the individual of each classification value.

The anthropologists also mentioned in their observation that most of the models were deformed post-mortem causing an imperfect fit. This could be reversed on the acquired 3D models in order to obtain an even better reconstruction, however this is a very complex process and thus beyond the scope of this project.



# 7 CONCLUSION AND FUTURE WORK

---

## 7.1 Conclusion

The CraMs application's goal is to provide a better alternative to the traditional methods used by the anthropologists. CraMs improvements upon these methods by reducing measurement errors, allowing for analysis to be done remotely without physically manipulating the skull reducing the risk of damage, improving overall speed of the anthropologist's workflow and providing types of analysis that could be done otherwise.

The fragment reconstruction method even though it went through significant evolutions during development was hampered by not being able to use more traditional solutions found in literature still produced great results. The initial rough alignment created could not be fully automated but the three different solutions (using pairs of points with just the fragments, with a template or direct manipulation of the fragments) provide good alignments with little work while being optimized for different types of situations. The fracture matching method was the main advancement. It provided an innovative solution that calculated transformation matrix while remaining very fast which would allow room for the process to be enhanced in and tackling new types of fragments in the future. The solution works perfectly with large fragments and was not tested with smaller ones because none were available. Theoretically there should be no problem with other because the underlying fundamentals are still the same: fracture has a mostly constant curvature is distributed on the outside edges of each fragment.



The Ancestry Estimation process started very much as an improvement on speed/convince. The anthropologists desired a way for to quickly and accurately estimate the ancestry of the individual being analyzed. The solution implemented showed very positive results like the one provided by 3D-ID, the application whose features were desired by the experts. Additionality with the dataset used in process being an ever-growing resource with each use of the application the effectiveness of this solution will only increase. The contributions made here can also be repurposed in different area of morphologic analysis using the centralized database as a source.

## 7.2 Future Work

CraMs, as every other application can always be improved upon. Some of the relevant improvements we devised are:

- Replace the ICP based solution for the initial skull alignment with a method using keypoint and descriptor scheme, like the one described in section 5.1.1. This method is superior in performance and much more robust and since were dealing with complete models that are “thin-shelled”, isn’t subject to the same problems as those faced in the fragment reconstruction.
- Create new system to estimate the position of every point by taking advantage of the craniometric database. With the large set of point data points can be estimated roughly based on the average position on an aligned skull. The anthropologists would then only need to correct the position of these points, massively speeding up the point marking process which is the time-consuming part of the process.
- The acquisition of skulls fragments can vary from difficult to outright impossible depending on their size. A solution to create 3D models using MRI scans as an acquisition method would be a step in the right direction to reconstruct skulls with more numerous fragments and would allow more skulls to be added, enrichening the data set.
- The reconstruction process was somewhat hindered by having the rough pre-alignment needing a lot of user input. This could be improved by calculating color or pattern similarities between fragments textures to deduce the preliminary alignment.

- Streamlining the CraMs code base by simplifying the messy code that is added in every iteration and removing redundancies that make it very hard to read for someone getting started with this project. Additionally, documentation should be created in conjunction with a style guide for future work.
- Calculate craniometric measurements by manipulating the Phantom Omni tool on a physical skull to analyze it with the need to 3D Scanner acquisition.



# REFERENCES

---

- Andrade, B. (2016). CraMs: Application for geometry analysis of skulls using 3D models. *Master Dissertation, Universidade de Aveiro*.
- Balzeau, A., Crevecoeur, I., Rougier, H., Froment, A., Gilissen, E., Grimaud-Hervé, D., Semal, P. (2010). Applications of imaging methodologies to paleoanthropology: Beneficial results relating to the preservation, management and development of collections. *Comptes Rendus Palevol*, 9(6–7), 265–275. Retrieved from <http://doi.org/10.1016/j.crpv.2010.07.006>
- Besl, P. J., & McKay, H. D. (1992). A method for registration of 3-D shapes. *IEEE Transactions on Pattern Analysis and Machine Intelligence*, 14(2), 239–256. Retrieved from <http://doi.org/10.1109/34.121791>
- Buck, T. J., & Vidarsdottir, U. S. (2004). A proposed method for the identification of race in sub-adult skeletons: a geometric morphometric analysis of mandibular morphology. *Journal of Forensic Sciences*, 49(6), 1159–1164. <http://doi.org/10.1520/JFS2004074>
- Coelho, C. R. S. (2012). *Uma identidade perdida no mar e reencontrada nos ossos : Avaliação das afinidades populacionais de uma amostra de escravos dos séculos XV-XVI. Master Dissertation, University of Coimbra*.
- Du, G., Zhou, M., Yin, C., Wu, Z., & Shui, W. (2016). Classification and reassembly of archaeological fragments. *Proceedings of the Symposium on VR Culture and Heritage - VRCAI '16*, 67–70. <http://doi.org/10.1145/3014027.3014031>
- Everson, R. (1997). Orthogonal , but not Orthonormal , Procrustes Problems. *Convergence*, (4), 1–11.
- Ferreira, M. T., Vicente, R., Navega, D., Gonçalves, D., Curate, F., & Cunha, E. (2014). A new forensic collection housed at the University of Coimbra, Portugal: The 21st century identified skeletal collection. *Forensic Science International*.
- Fischler, M. a, & Bolles, R. C. (1981). Random Sample Consensus: A Paradigm for Model Fitting with. *Communications of the ACM*, 24, 381–395. <http://doi.org/10.1145/358669.358692>

- G. N. van Vark and W. W. Howells, E. (1984). *Multivariate Statistical Methods in Physical Anthropology*. Springer Netherlands.
- Gower, J. C. (1975). Generalized procrustes analysis. *Psychometrika*, 40(1), 33–51. <http://doi.org/10.1007/BF02291478>
- Hefner, J. T. (2009). Cranial Nonmetric Variation and Estimating Ancestry. *Journal of Forensic Sciences*, 54(5), 985–995.
- Howells, W. W. (1973). Cranial Variation in Man -A study by multivariate analysis of patterns of difference among recent human populations. *Papers of the Peabody Museum of Archaeology and Ethnology*, 67, 1–259.
- Johnson, A. E., & Hebert, M. (1999). Using spin images for efficient object recognition in cluttered 3D scenes. *IEEE Transactions on Pattern Analysis and Machine Intelligence*, 21(5), 433–449. <http://doi.org/10.1109/34.765655>
- Kampel, M., Sablatnig, R. (2000). Color classification of archaeological fragments. *Pattern Recognition, International Conference on 4*, 4771.
- Kendall, D. G. (1989). A Survey of the Statistical Theory of Shape. *Statistical Science*, 4(2), 87–99. Retrieved from [http://www.jstor.org/stable/2245331?seq=1#page\\_scan\\_tab\\_contents](http://www.jstor.org/stable/2245331?seq=1#page_scan_tab_contents)
- Neves, L. (2014). *Measures and detection of morphology for craniometry using 3D models*. Master Dissertation. Universidade de Aveiro.
- Orlov, A. I. (2011). Mahalanobis distance. In *Encyclopedia of Mathematics* (p. 1). Retrieved from [http://www.encyclopediaofmath.org/index.php?title=Mahalanobis\\_distance&oldid=17720](http://www.encyclopediaofmath.org/index.php?title=Mahalanobis_distance&oldid=17720)
- Pauly, M., Keiser, R., & Gross, M. (2003). Multi-scale Feature Extraction on Point-Sampled Surfaces. *Computer Graphics Forum*, 22(3), 281–289. <http://doi.org/10.1111/1467-8659.00675>
- Pereira, C., & Mello e Alvim, M. (1979). *Manual Para Estudos Craniométricos E Cranioscópicos*. (Univ. Federal de Santa Maria, Ed.).
- Perini, T. A., Oliveira, G. L. De, Ornellas, S., & Oliveira, F. P. De. (2005). Technical error of measurement in anthropometry. *Revista Brasileira de Medicina Do Esporte*, 11, 86–90.
- Rusu, R. B., Blodow, N., & Beetz, M. (2009). Fast Point Feature Histograms (FPFH) for 3D registration. In *2009 IEEE International Conference on Robotics and Automation* (pp. 3212–3217). <http://doi.org/10.1109/ROBOT.2009.5152473>
- Sablatnig, R., Menard, C., Kropatsch, W. (1998). Clas- sification of archaeological fragments using a description lan- guage. In *Signal Processing Conference (EUSIPCO 1998)*,.
- Salti, S., Tombari, F., & Di Stefano, L. (2014). SHOT: Unique signatures of histograms for surface and texture description. *Computer Vision and Image Understanding*, 125(September), 251–264. <http://doi.org/10.1016/j.cviu.2014.04.011>

- Santos, D. (2013). 3D skull models : a new craniometric approach. *Master Dissertation, Universidade de Aveiro*.
- Schönemann, P. H. (1966). A generalized solution of the orthogonal procrustes problem. *Psychometrika*.  
<http://doi.org/10.1007/BF02289451>
- Slice, D. E., & Ross, A. (2009). 3D-ID: geometric morphometric classification of crania for forensic scientists. Retrieved from <http://www.3d-id.org>
- Stephens, C. (2000). A Measure of Truth ? An Examination of the History , Methodology , Theory and Practice of Craniometric Analysis : With Special Focus on its Application in Forensic Identification. *Totem: The University of Western Ontario Journal of Anthropology*, 8(1).
- Vieira, M., & Shimada, K. (2005). Surface mesh segmentation and smooth surface extraction through region growing. *Computer Aided Geometric Design*, 22(8), 771–792. Retrieved from <http://doi.org/10.1016/j.cagd.2005.03.006>
- Wachowiak, M. J. wachowiakm si edu, & Karas, B. V. karasb si edu. (2009). 3D Scanning and Replication for Museum and Cultural Heritage Applications. *Techniques de Balayage et de Reproduction En Trois Dimensions Pour Applications Muséales et 89 Culturelles.*, 48(2), 141–158. Retrieved from <http://doi.org/10.2307/27784660>
- Wasterlain SN, Neves MJ, F. M. (2016). Dental modifications in a skeletal sample of enslaved Africans found at Lagos (Portugal). *International Journal of Osteoarchaeology*, 26, 621–632.
- Weber, G. W. (2013). Another link between archaeology and anthropology: Virtual anthropology. *Digital Applications in Archaeology and Cultural Heritage*, 1(1), 3–11. Retrieved from <http://doi.org/10.1016/j.daach.2013.04.001>
- Yin, Z., Wei, L., Li, X., & Manhein, M. (2011). An automatic assembly and completion framework for fragmented skulls. *Proceedings of the IEEE International Conference on Computer Vision*, (1), 2532–2539. <http://doi.org/10.1109/ICCV.2011.6126540>
- Yu, Z. (2009). Intrinsic shape signatures: A shape descriptor for 3D object recognition. *2009 IEEE 12th International Conference on Computer Vision Workshops, ICCV Workshops 2009*, (November 2009), 689–696. <http://doi.org/10.1109/ICCVW.2009.5457637>
- Zhang, K., Yu, W., Manhein, M., Waggenspack, W., & Li, X. (2015). 3D Fragment Reassembly Using Integrated Template Guidance and Fracture-Region Matching. *2015 IEEE International Conference on Computer Vision (ICCV)*, 2138–2146. <http://doi.org/10.1109/ICCV.2015.247>



# ANNEX A – CRAMS USER MANUAL

---

This annex serves as a manual for the usage CrAMs with incidence on the features created during dissertation. The manual for other CrAMs tools can be view in the previous dissertations (Andrade, 2016; Neves, 2014; Santos, 2013).

## Ancestry Menu

This menu, shown in Figure 1 contains the Ancestry Estimation tools and database management.

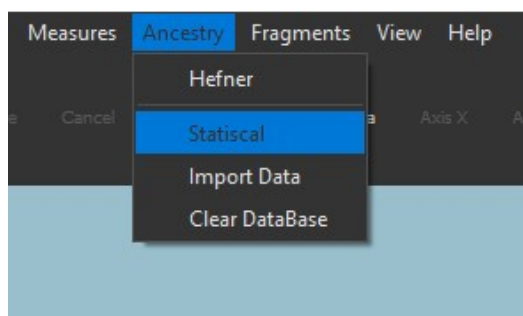


*Figure 1 – Ancestry Menu.*

- The previous Ancestry Estimation process created by (Andrade, 2016) was moved here from the Structures menu and renamed Hefner.
- “Statistical” contains the Ancestry Estimation process developed in this dissertation.
- “Import Data” allows the addition of new data to the Craniometric Point Database from a .csv file.
- “Clear Database” deletes all the data in the Point Database.



## Statistical Ancestry Estimation

1. Load a model.
2. Align the model using any of the tools available.
3. Mark the craniometric points on the model.
4. Select Statistical from the Ancestry menu.
5. The resulting classification and auxiliary metrics are displayed in a window as shown in Figure 2.

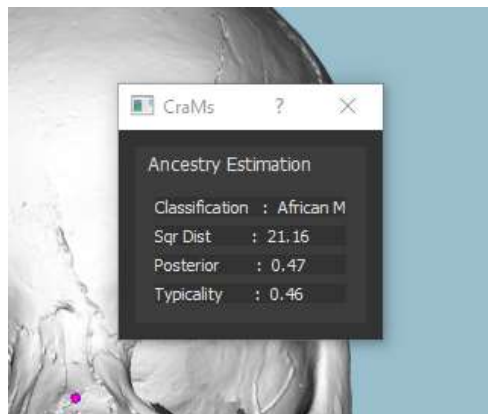


Figure 2 – Statistical Ancestry Estimation results.

## Load Multiple Fragments

To accommodate the Fragment Reconstruction, process an option to load multiple model with the title "Load Fragments" as shown in Figure 3.

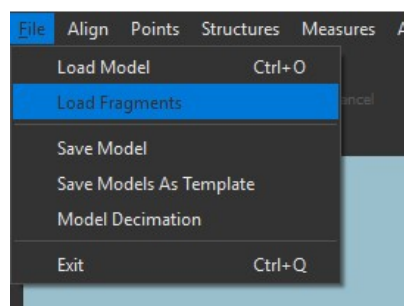


Figure 3 – Load Fragments option in the File Menu.

## Fragments Menu

The fragment menu, seen in Figure 4 and Figure 5, holds the methods to perform a reconstruction. It contains two sub-menus for each of the two phases outlined in Chapter 5: “Pre-Alignment” and “Refinement”.

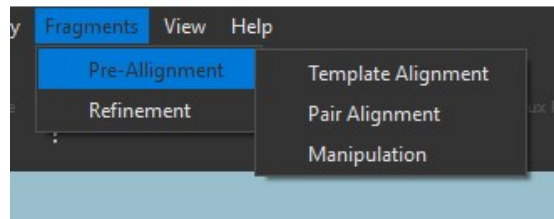


Figure 4 – Pre-Alignment sub-menu.

The “Pre-Alignment” sub-menu contains three options:

- “Template Alignment” which contains the alignment through point pairs with the fragments and a template.
- “Pair Alignment” which contains the alignment through point pairs with the pairs of fragments.
- “Manipulation” which contains the manual alignment done by moving the fragments directly.

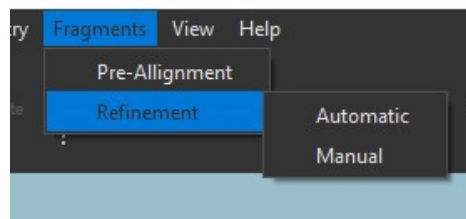


Figure 5 – Refinement sub-menu.

The “Refinement” sub-menu contains two options:

- “Automatic” which contains the fracture region based alignment refinement where this region is calculated automatically.

- “Manual” which the same alignment refinement process but the fracture region is obtained with human interaction.

## Fragment Reconstruction

1. Load the Fragment Models into Crams
2. Align the fragments using one of the option in the “Pre-Alignment” sub-menu.
  - a. Template Alignment as seen in Figure 6:
    - i. Select the template model file to load it.
    - ii. Use the ‘P’ hotkey or press the “Pick Points” button.
    - iii. Select equivalent points between the fragments and the template.
    - iv. Click the “Validate” button to generate the alignment.

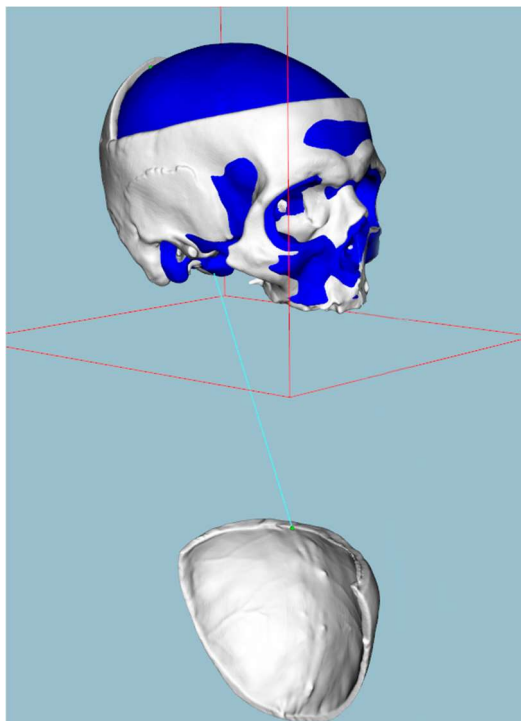


*Figure 6 – Template Pre-Alignment.*

- b. Par Alignment:
    - i. Use the 'P' hotkey or press the "Pick Points" button.
    - ii. Select equivalent points between the fragments.
    - iii. Click the "Validate" button to generate the alignment.
  - c. Manipulation
    - i. Move the fragments to position by clicking and dragging with the middle mouse button and rotating it with left mouse button.
    - ii. Click the "Validate" button to generate the alignment.
3. Perform a higher precision alignment using one of the option in the "Refinement" sub-menu.
- a. Automatic Refinement, as seen in Figure 7.
    - i. Inspect the generated fracture region.
    - ii. Click the "Validate" button to complete the reconstruction.

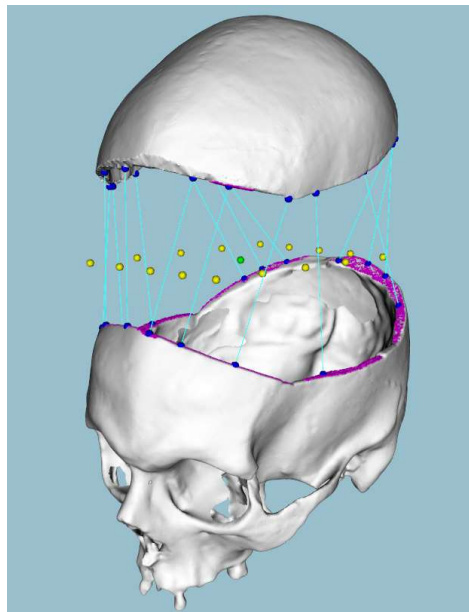


*Figure 7 – Automatic Fracture region.*

b. Manual Refinement as seen in Figure 8

- i. Use the 'P' hotkey or press the "Pick Points" button.
- ii. Click on a point in the fracture region to be expanded.
- iii. When the fracture regions of the fragments are covered click the "Validate" button or used the "v" keyboard shortcut to complete the reconstruction.

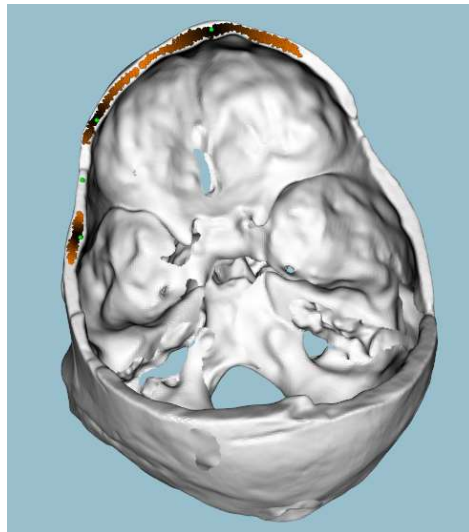


*Figure 8 – Manual Fracture region.*

# ANNEX B – INSTALATION GUIDE

---

In this annex, the installation process for the necessary dependencies required by CraMs project is described.

The CraMs project was developed using Visual Studio 2015 and used the following libraries:

- VTK 7.0.0
- Qt 5.7.0
- OpenCV 3.1.0
- WildMagic 5.14
- Boost 1.55.0
- CMake 3.6.2

However, any other versions of these libraries can be used by configuring the file paths during the CMake generation process. In the following section the installation process for windows will be described. Note that all the libraries must be built with the same mode to be used with CraMs, DEBUG or RELEASE and the code generation must set to “Multi-thread MT”.

## Windows Installation Process

1. Install CMake minimum version 2.6.
2. Install Qt minimum version 4.8.
3. Create a system environment variable named “QTDIR” and set it to the QT installation folder. Edit the “Path” variable and add the path to the “bin”, “lib”, “include” folders inside the QT folder.

4. Extract OpenCV files and open both “build” and “sources” in CMake.
5. Add “OPENCV\_DIR” environment variable and set the value to the OpenCV “build” folder. Edit the “Path” variable and add the path to the “build” and the “bin” for your Visual Studio version and CPU architecture as seen in Figure 1.

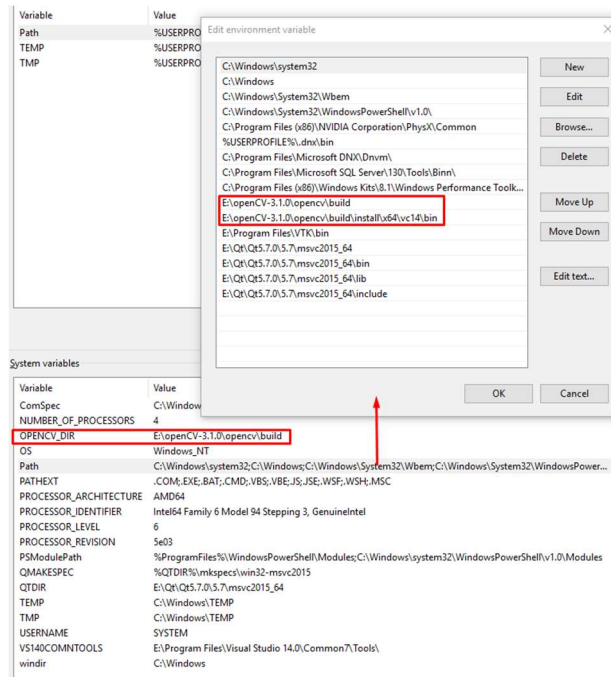


Figure 1 – Windows Environment Variables for OpenCV.

6. On CMake Click configure, select your Visual Studio compiler and generate.
7. Build the resulting OpenCV solution with Visual Studio.
8. Extract VTK source files and create a build folder.
9. Open both folders with CMake and configure it for your compiler.
10. Make sure *VTK\_Group\_Qt*, *VTK\_Group\_Rendering* and *VTK\_Group\_View* are ticked and select your Qt and OpenGL versions as shown in Figure 2.

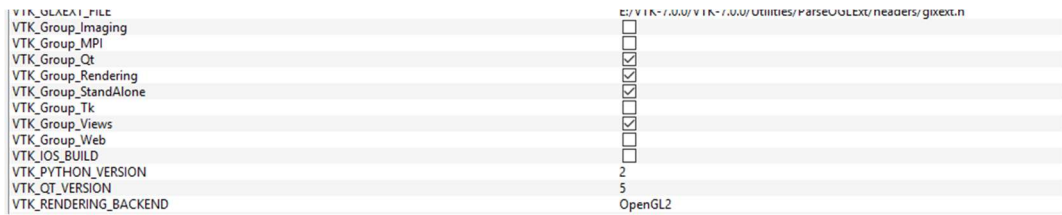


Figure 2 – VTK options in CMake.

11. Select Advanced Setup and then enable the options `Module_vtkGUISupportQtOpenGL` and `Module_vtkGUISupportQtWebKit` as shown in Figure 3.



Figure 3 – VTK GUI advanced options in CMake.

12. Generate in CMake.
13. In Visual Studio set all the library's code generation to "Multi-thread MT" and build it.
14. Add VTK "bin" sub folder to system "Path" variable.
15. Extract WildMagic and build it with Visual Studio.
16. Extract Boost and build it with Visual Studio.
17. Create a CraMs project folder with a "build" and "source" sub-folder.
18. Run CMake and set build and source folders for the project.
19. Click configure and select your compiler.
20. Set paths for the BOOST\_DIR, WM5\_CORE\_LIB and WM5\_MATH\_LIB entries.
21. Generate and build resulting solution.
22. Add the sqlite3.dll to the Release/Debug folder.



All the required dependencies should now be linked in the Visual Studio project. The configuration must be set to the same setting as the dependencies (DEBUG/RELEASE). Additionally, the code Generation mode should be set to the same option used in the dependencies, "Multi-thread MT".

## ANNEX C – POINTS OF INTEREST

---

The figures present in this annex were taken from (Pereira & Mello e Alvim, 1979). The following section described the feature points used, their abbreviation and how they are defined:

- 1 Alveolon (alv): intersection point of the mid line of the palate with the perpendicular tangent to the posterior border of the alveolar arch;

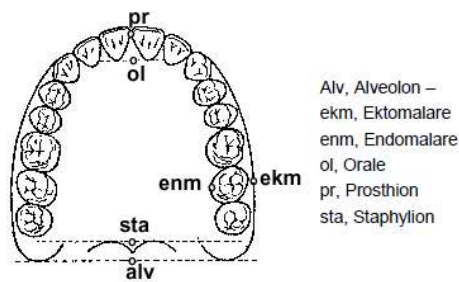
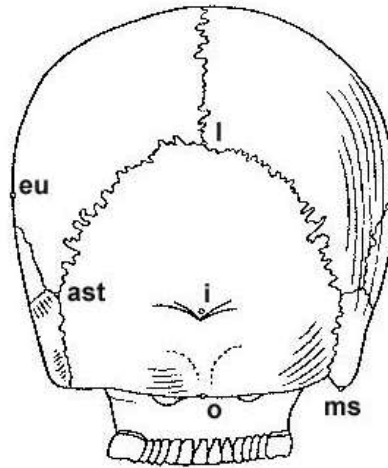


Figure 1 – Palatal Arch.

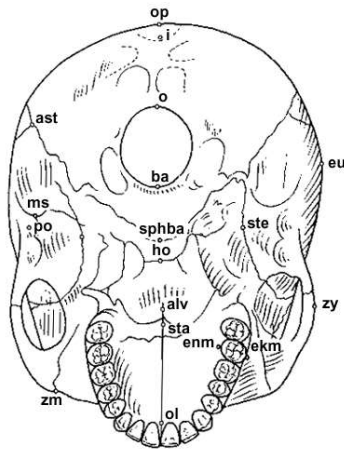
- 2 Basion (ba): the point is situated on middle border of the anterior margin of the foramen magnum. This feature point is defined as the point with minimum Y coordinate in the Z axis (considering a threshold of  $\pm 0.01$  mm in X and  $\pm 10$  mm in Z coordinates);
- 3 Bregma (b): intersection point between the sagittal suture and the coronal suture. The algorithm selects a starting point as the coordinate with greater Y value on the region of points of X and Z within a  $\pm 0.01$  mm threshold. Then, it analyses neighbour points in order to find a discontinuity in the Y values, i.e., sudden smaller followed by higher Y values with the aim of finding the coronal suture. Once the suture region is found, the Bregma is selected as point in the region with smaller Y coordinate;



Ast, Asterion – eu, Eurion – i, Inion – l, Lambda – mas, Mastoidale – o, Opisthion.

Figure 2 - Skull back view.

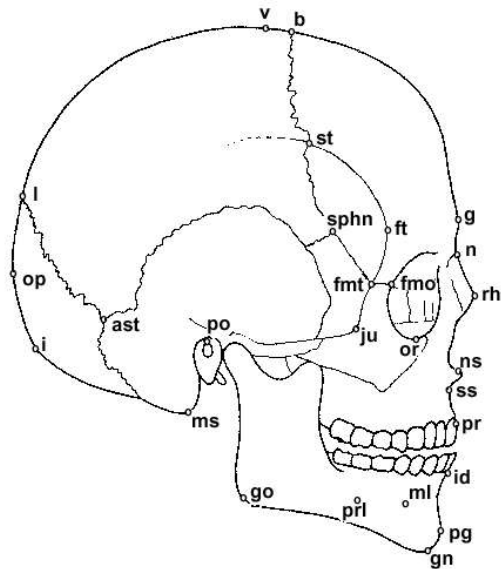
- 4 Dakyon (d): point located at the apex of the angle formed by the frontolacrimal suture and lacrimomaxilar suture;
- 5 Ektokonchion (ek): Point located on the outer edge of the orbit and the furthest possible of the *maxillofrontale* point;
- 6 Ektomalare (ekm): Point situated in the palatal surface of the alveolar arch, in the middle portion of the second molar;
- 7 Eurion (eu): Most lateral point of the *neurocranium*. Has no fixed location and varies from one individual to another and from one population to another;
- 8 Frontotemporale (ft): most anterior point of the temporal line, located approximately at the root of the zygomatic apophysis of the frontal bone;
- 9 Frontomolare-Temporale (fmt): point most posterior and lateral of the frontomalar suture, in the temporal region;
- 10 Glabella (g): Point located just above the frontonasal suture, between the superciliary arches. Commonly is the most salient point of the front, in the sagittal plane. It may, however, constitute or form a depression, with the superciliary arch (a single continuous elevation);



alv, Alveolon - ast, Asterion - ba, Basion - ekm, Ektomalare - enm, Endomlare - eu, Eurion - ho, Hormion - l, Inion - ms, Mastoideale - o, Opisthion - op, Opisthokranion - ol, Orale - po, Porion - sphba, Sphenobasion - sta, Staphylion - ste, Stenion - zy, Zygon - zm, Zygomaxillare.

Figure 3 - Skull bottom view.

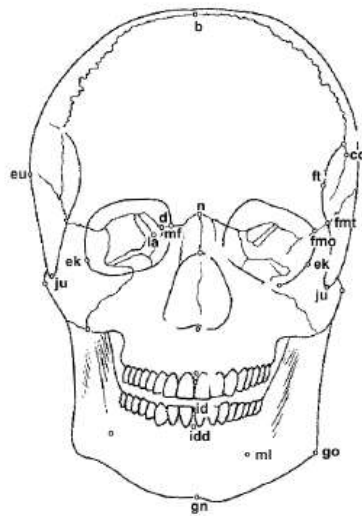
- 11 Lambda (l): Intersection point between the sagittal and lambdoid sutures;
- 12 Mastoidale (ms): Lowest point of the mastoid process of the temporal;
- 13 Nasion (n): Intersection point of the frontonasal suture and suture internasal. Corresponds to the root of the nose;
- 14 Nasospinale (ns): Lowest point in the inferior edge of the piriform aperture at the base of the nasal spine, designed in the Sagittal Plane. This point is called by some authors Subnasale or Nasale;
- 15 Opisthion (o): Middle point of the posterior edge of the occipital hole;
- 16 Opisthokranion (op): Point that is the furthest from the *glabella* in sagittal plane of the occipital. Sometimes coincides with the *inion*. There are cases where this occipital region is more or less flat;



ast, Asterion - b, Bregma - fmo, Frontomale orbitale - fnt, Frontomale temporale - ft, Frontotemporale - g, Glabella - gn, Gnathion - go, Gonion - i, Inion - id, Infradentale - ju, Jugale - l, Lambda - ms, Mastoidale - ml, Mentale - n, Nasion - ns, Nasospinale - op, Opisthokarion - or, Orbitale - pg, Pogonion - po, Porion - pri, Prominentia laterale - pr, Prosthion - rhi, Rhinion - sphn, Sphenion - st, Stephanion - ss, Subspinale - v, Vertex

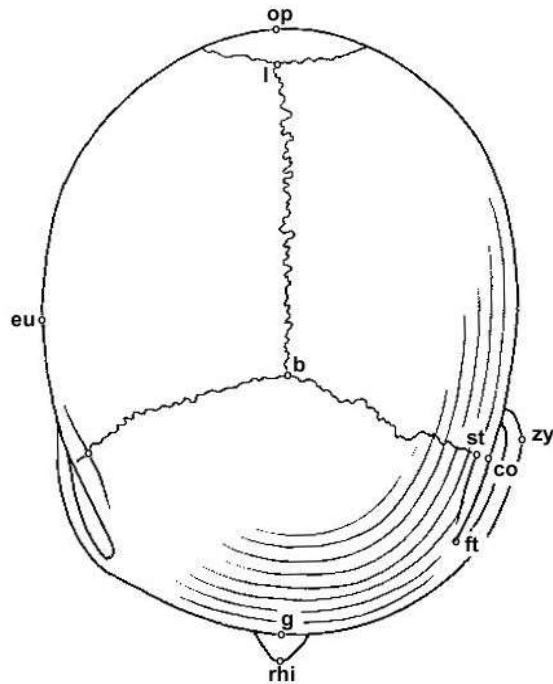
*Figure 4 - Skull side view.*

- 17 Porion (po): Point on the upper and outer border of the external auditory canal;
- 18 Prosthion (pr): Most anterior point of the alveolar ridge between the central incisors.  
Corresponds to the lower end and anterior interalveolar septum in the sagittal plane;
- 19 Vertex (v): Highest point of the skull located in the sagittal suture and in the Frankfurt plane;
- 20 Zygion (zy): Most lateral point of the zygomatic arch, on each side. Given the aligned skull both Zygion are defined as the points with maximum and minimum X coordinates, respectively to the right and left points. Since the zygomatic arch might not be the largest zone of the skull, we only consider the portion of the skull with negative Y values;
- 21 Zygomaxillare (zm): Lowest point of the maxilomalar suture.



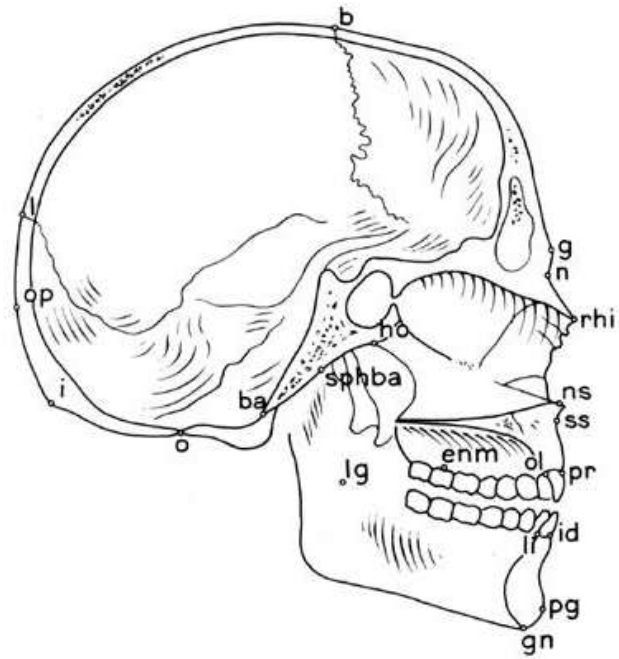
b, Bregma – co, Coronale – d, Dakyon – ek, Ektokonchion – eu, Eurion – fmo, Frontomalare orbitate- fnt, Frontomalare temporale – ft, Frontotemporale – gn, Gnathion – go, Gonion – id, Infradentale – idd, Infradentale dentale – ju, Jugale – la, Lacrimale – mf, Maxillofrontale – ml, Mentale – n, Nasion – ns, Nasospinale – or, Orbitale – prl, Prominentia laterale – pr, Prosthion – prd, Prosthion dentale – rhi, Rhinion – st, Stephanion – zy, Zygion – zm, Zygomaxillare

Figure 5 - Skull front view.



b, Bregma – co, Coronale – eu, Eurion – ft, Frontotemporale – g, Glabella – l, Lambda – op, Opisthokranion – rhi, Rhinion – st, Stephanion – zy, Zygion

Figure 6 - Skull top view.



Ba, Basion - b, Bregma - enm, Endomalare - g, Glabella - gn, Gnathion - ho, Hormion - i, Inion - id, Infradentale - l, Lambda - li, Linguale - lg, Lingulare - n, Nasion - ns, Nasospinale - o, Opisthion - ol, Orale - op, Opisthokranion - pg, Pogonion - pr, Prosthion - rhi, Rhinion - spha, Sphenobasion - ss, Subspinale.

*Figure 7 - Skull side cut view.*

## ANNEX D – CRANIOMETRIC MEASURES

The iDryas team used 24 measures to classify the skulls. In this annex these measures are listed, along with their definition and representative images taken from the master thesis of Catarina Coelho (Coelho, 2012), one of the team's specialists.

- 1 ZYB (bizygomatic width): the distance between both *Zygion* points;
- 2 BBH (*Basion-Bregma* height): distance between *Basion* and *Bregma*;
- 3 XCB (maximum skull width): maximum width perpendicular to the sagittal plane;
- 4 GOL (maximum skull length): distance (straight line) between *Glabella* and *Opisthokranion*;
- 5 BNL (*Nasion-Basion* length): distance between *Basion* and *Nasion*;





6 FRC (frontal line): distance, in the sagittal plane, between the *Nasion* and *Bregma*;



7 BPL (*Basion-Prosthion* length): the distance (strait line) between *Basion* and *Prosthion*;



8 UFHT (superior facial height): distance between *Nasion* and *Prosthion*;



9 MAB (*maxillo-alveolar* width): is the maximum width of the alveolar arch on the outer surface (the distance between both *Ektomalare* points);



10 AUB (*Biauricular* width): the minimum exterior width measured in the root of the zygomatic processes;



11 NLH (nasal height): distance between the *Nasion* and *Nasospinale*;



12 UFBR (superior facial width): distance between both *Frontomolare-Temporale* points;



13 PAC (parietal line): distance, in the sagittal plane, between *Bregma* and *Lambda*;



14 FOL (length of the *Foramen Magnum*): distance between *Basion* and *Opisthion*;



15 WFB (minimum facial width): distance between both *Frontotemporale* points;



16 NLB (nasal width): maximum width of the nasal aperture;



17 OBB (orbital width): distance between *Dakyon* and *Ektokonchion*;



18 EKB (bi-orbital width): distance between both *Ektokonchion points*;



19 DKB (inter-orbital width): distance between both *Dakyon points*;



20 OCC (occipital line): distance, in the sagittal plane, between *Lambda* and *Opisthion*;



21 FOB (width of the *Foramen Magnum*): distance between the lateral margins of the *Foramen Magnum*, in the lateral point with biggest curvature;



22 MAL (*maxillo-alveolar* length): distance between the *Prosthion* and *Alveolon*;



23 MDH (height of the *Mastoid process*): distance, in projection, between the *Frankfurt plane* and the nadir point of the *Mastoid process*;



24 OBH (orbital height): distance between the border of the inferior and superior orbit.

